Article

Distributed Lyapunov-Based Model Predictive Control for AUV Formation Systems with Multiple Constraints

Zheping Yan, Mingyao Zhang *, Jiajia Zhou and Lidong Yue

College of Intelligent Systems Science and Engineering, Harbin Engineering University, Harbin 150001, China; yanzheping@hrbeu.edu.cn (Z.Y.); zhoujiajia@hrbeu.edu.cn (J.Z.); yuelidong@hrbeu.edu.cn (L.Y.)
* Correspondence: zhangmingyao@hrbeu.edu.cn

Abstract: This paper focuses on the formation tracking issue of autonomous underwater vehicles (AUVs) subject to multiple constraints in three-dimensional space. We developed a novel distributed Lyapunov-based model predictive controller (DLMPC) with a fast finite-time extended state observer (FFTESO). Initially, the external disturbances and internal uncertainties of each AUV were precisely compensated using the designed FFTESO. Subsequently, we proposed DLMPC-based position tracking and velocity tracking controllers, which solved an online optimization problem to determine optimal velocities and control forces. This hierarchical framework effectively managed system constraints, such as state constraints and actuator saturation. Additionally, the Lyapunov-based backstepping control law was applied to construct stability constraints in the distributed optimization problem, ensuring the recursive feasibility and closed-loop system stability of the proposed scheme. Sufficient conditions and attraction regions to ensure stability were explicitly provided. Finally, the simulation results demonstrated that the proposed method improved both the convergence speed and tracking accuracy by at least 30% compared to other methods.

Keywords: autonomous underwater vehicles; finite-time extended state observer; distributed Lyapunov-based model predictive control; formation trajectory tracking; multiple constraints

1. Introduction

Due to their critical role in undersea exploration and hydrographic observation, autonomous underwater vehicles (AUVs) have emerged as the most effective tools for ocean development thus far [1]. In contrast to the limitations of individual AUVs, multi-AUV systems offer a broader detection range, heightened operational efficiency, and enhanced redundancy performance. Given these significant advantages, research on AUV formation control has garnered increasing attention [2]. The primary challenge is to ensure the stability of the formation motion in intricate underwater environments with multiple constraints [3]. Addressing this issue, researchers have undertaken extensive studies in recent years. A behavioral decision-making-based path planning method for AUVs was proposed in [4], but the built-in model creates challenges for mathematical analysis. The leader–follower method, introduced for AUV formation tracking control in [5], confronts challenges related to poor robustness and fault tolerance due to the presence of a designated leader. Consequently, there has been a growing focus on the more promising leaderless formation approach [6]. In [7], a virtual structure-based method for AUV formation control was developed, but its flexibility and applicability are constrained. Despite substantial research in this domain, crafting a control scheme that provides optimal control performance while accommodating multiple constraints remains a primary research objective for multi-AUV systems.

The most typical constraints are the various disturbances encountered by AUVs. These include internal disturbances within the system, such as model uncertainties caused by coupled dynamics and varying system parameters [8]. Another significant factor is the unpredictable external disturbances caused by currents in the actual ocean environment [9].

Additionally, system constraints impose considerable challenges on AUV formation motion. For instance, the cruising speed and attitude angle of an AUV are subject to specific limitations [10]. These intrinsic state constraints place substantial demands on the design of the controller. Furthermore, actuator saturation constraints are a pertinent concern in real applications, stemming from limitations in the active drive force due to the physical characteristics of the actuator. If the control inputs violate this limit, it will degrade the control performance of the system [11]. The traditional control methods in the aforementioned studies have difficulty in achieving optimal control performance. In contrast, model predictive control (MPC) offers notable advantages in explicitly managing system constraints and optimizing performance [12]. It has found widespread application in various control systems subject to multiple constraints. In terms of AUV formation control, distributed model predictive control (DMPC) has garnered increased attention among researchers. As a result, there is an urgent need to provide an AUV formation control strategy that guarantees closed-loop system stability under external disturbances, internal model uncertainties, and system constraints.

In response to the above facts and challenges, we propose a novel FFTESO-based hierarchical DLMPC strategy for AUV formation tracking systems subject to multiple constraints in the complex ocean environment. The scheme precisely compensates for lumped disturbances while concurrently accounting for system constraints, such as actuator saturation and state constraints. The Lyapunov-based backstepping method is employed to ensure closed-loop stability.

The subsequent sections of this paper are organized as follows. Section 2 overviews related works on responses to multiple constraints and MPC. Section 3 presents the AUV modeling and problem formulation. Section 4 proposes the methodology, including the design of the FFTESO and DLMPC-based hierarchical tracking controllers, as well as the theoretical analysis of the system stability. In Section 5, the comparative simulation results are demonstrated. Finally, conclusions are drawn in Section 6.

2. Related Work

In recent decades, to enhance the robustness and adaptability of formation control systems against disturbances, diverse advanced methods have been explored. These encompass disturbance observers [13], adaptive control methods [14], and strategies involving neural networks [15]. Notably, the extended state observer (ESO) stands out due to its superior property of not requiring precise information about the controlled object. In recent years, the ESO technique proposed in [16] has demonstrated potential for disturbance compensation. It treats internal uncertainties and external environmental disturbances as lumped disturbances, extending them into a new state. In [17], an output feedback motion control method employing a high-gain ESO was developed. This method effectively compensates for measurement errors, external disturbances, and model uncertainties in remotely operated vehicles. Additionally, Ref. [18] introduced AUV tracking controllers based on a generalized ESO and a harmonic ESO, which are intended to ensure path tracking even in the presence of lumped disturbances. Despite the diversity of ESOs developed by researchers, their capability is often constrained to ensuring asymptotic convergence on the observation error without effectively limiting the convergence time. To enhance higher estimation accuracy in complex environments, there is a growing attraction towards finite-time ESO.

The design strategy for conventional FTESOs is presented in [19] and the estimation of the convergence time under different cases is given for the first time. A robust fault-tolerant controller based on FTESO was designed in [20] to estimate the lumped disturbances of spacecraft. The control algorithm incorporates nonsingular terminal sliding mode and super-twisting methods. The authors of [21] investigated a safety control based on the FTESO adaptive neural network for unmanned aerial vehicles. The double-power FTESO was utilized to compensate for lumped disturbances. Nevertheless, there is room for further optimization of the observer's structure to enhance compensation performance.

To cope with actuator saturation and state constraints, an adaptive energy-saving trajectory tracking control strategy for AUVs was proposed in [22]. A compensator based on radial basis function neural network was used to solve the problems of saturation of the actuator and multi-objective optimization. In [23], an adaptive super-twisting algorithm-based sliding mode controller (ASTASMC) was introduced for the formation control problem in a multi-AUV recovery system. This controller utilizes a robust adaptive law to estimate unclear hydrodynamic parameters and unknown environmental disturbances in real time.

DMPC addresses constrained optimization problems based on information from the AUV itself and its neighboring vehicles. In [24], a DMPC-based formation tracking method for AUV systems subject to input constraints was introduced. However, it is important to note that this approach solely considered the kinematics of the AUV and did not support a realistic AUV model. Addressing the AUV formation control under compound disturbances, Ref. [25] proposed a FTESO-based dual closed-loop DMPC scheme. However, stability analysis for optimal control problems within a finite horizon has proved challenging, often requiring the addition of suitable terminal constraint sets or selecting sufficiently large prediction horizons [26]. To overcome these limitations, a Lyapunov-based MPC (LMPC) method was proposed in [27], ensuring the stability of the control system through the construction of Lyapunov contraction constraints. This method inherits the stability and robustness of the Lyapunov-based control law, offering valuable insights for the design of AUV formation controllers. Based on stochastic Lyapunov feedback control strategies, Ref. [28] developed a Lyapunov-based MPC method for nonlinear systems subject to stochastic uncertainties. The authors of [29] studied iterative DMPC method for large-scale nonlinear systems subject to asynchronous and delayed state feedback. The stability constraints of the iterative DMPC were formulated by utilizing the Lyapunov-based control technique. To the best of our knowledge, a Lyapunov-based distributed predictive control law was only proposed in [30] to solve the three degrees-of-freedom (DOF) AUV formation tracking issue under time-varying disturbances. However, its applicability is limited to plane motion and does not consider model uncertainties. The state-of-the-art methods related to DLMPC are summarized in Table 1.

Table 1. Comparison between state-of-the-art methods.

Methods	Applications	Main Contributions	Limitations
LMPC [27]	Trajectory tracking for AUVs	Stability constraints for LMPC systems of AUVs are given for the first time	The lumped disturbances are ignored and the closed-loop stability is conservative
Stochastic LMPC [28]	Nonlinear systems with unbounded stochastic uncertainties	Stability constraints are explicitly characterized in a probabilistic sense	Applicability and scalability can be further improved
Iterative DLMPC [29]	Nonlinear systems with asynchronous and delayed state feedback	Iterations can be terminated at any number without loss of closed-loop stability	Stability is limited by the dynamic behavior of the open-loop process
DLMPC [30]	Formation tracking for 3DOF AUVs	Contraction constraints are given for the stability of AUV disturbed formation	Only planar motion is considered and the control structure is simple

With respect to existing works, the principal contributions of this scheme include:

1. Compared with the existing DLMPC method [30], we have considered the lumped disturbances and improved the control structure. A hierarchical structure is employed, comprising a position controller and a velocity controller, aimed at generating the desired velocity and control force. This adaptation not only mitigates the challenge of

accessing the optimal solution but also augments the controllability of the velocity, thereby improving the spatial tracking accuracy of the formation system.

2. Compared to the FTESO utilized in [19,31], we have enhanced convergence speed by augmenting linear terms. This enables faster compensation of the disturbances for online updating of the prediction model. It not only enhances the estimation accuracy and convergence speed but also effectively mitigates the fluctuations of lumped disturbances. Hence, the robustness of the multi-AUV system is enhanced.

3. The Lyapunov-based backstepping control law is utilized to institute stability constraints within the DMPC problem. This choice ensures the recursive feasibility of the control algorithm and the stability of the closed-loop system. The conditions and attraction regions sufficient to ensure stability are explicitly given. The control performance of formation tracking is substantially improved.

3. Preliminaries

In this section, we present the AUV model and problem formulation, where a new version of the dynamic equation is demonstrated based on the task constraints.

3.1. AUV Modeling

The article selects a fully-actuated torpedo-type AUV from the literature [32] aligning with the task objectives. As shown in Figure 1, a 6DOF AUV is typically described by two reference frames: an earth-fixed frame $\{E\}$ and a body-fixed frame $\{B\}$. Since this AUV can be regarded as a highly metacentric stable vehicle with self-stable roll motion, we ignore the effect of roll; that is, roll angle $\phi_i = 0$, roll angular velocity $p_i = 0$, and the spatial motion of AUV is regarded as a 5DOF motion process. The kinematics and dynamics of the ith AUV are expressed as [33]:

$$\dot{\eta}_i = J_i(\eta_i)v_i \tag{1}$$

$$M_i\dot{v}_i + C_i(v_i)v_i + D_i(v_i)v_i + g_i(\eta_i) = \tau_i + \tau_{ic} \tag{2}$$

where $i = 1, 2, \ldots, N$, $\eta_i = [x_i, y_i, z_i, \theta_i, \psi_i]^T \in \mathbb{R}^5$ denotes the states of position and orientation of AUV, $v_i = [u_i, v_i, w_i, q_i, r_i]^T \in \mathbb{R}^5$ denotes the velocity states of the AUV. $J_i(\eta_i)$ is a rotation transformation matrix from the body-fixed frame to the earth-fixed frame and is assumed to be invertible (i.e., $|\theta_i| < \pi/2$), expressed as:

$$J_i(\eta_i) = \begin{bmatrix} \cos\psi_i\cos\theta_i & -\sin\psi_i & \cos\psi_i\sin\theta_i & 0 & 0 \\ \sin\psi_i\cos\theta_i & \cos\psi_i & \sin\psi_i\sin\theta_i & 0 & 0 \\ -\sin\theta_i & 0 & \cos\theta_i & 0 & 0 \\ 0 & 0 & 0 & 1 & 0 \\ 0 & 0 & 0 & 0 & 1/\cos\theta_i \end{bmatrix} \tag{3}$$

M_i denotes the inertial matrix. $C_i(v_i)$ and $D_i(v_i)$ represent the Coriolis and centripetal and hydrodynamic damping matrix, respectively. The gravitational and buoyancy forces of this AUV are balanced with each other such that the restoring force $g_i(\eta_i)$ is approximated to be zero. $\tau_i = [\tau_{iu}, \tau_{iv}, \tau_{iw}, \tau_{iq}, \tau_{ir}]^T$ denotes the control force and moment, and $\tau_{ic} = [\tau_{icu}, \tau_{icv}, \tau_{icw}, \tau_{icq}, \tau_{icr}]^T$ represents the time-varying unknown external disturbance. Specific expressions for these matrices are given in [34].

In practical applications, acquiring precise hydrodynamic coefficients for the AUV model might be challenging. It can generally be assumed that the coefficients are subject to certain perturbations ranging from -20% to 20% [35]. Thus, the parameter matrices are divided into $M_i = M_i^* + \Delta M_i$, $C_i(v_i) = C_i^*(v_i) + \Delta C_i(v_i)$, and $D_i(v_i) = D_i^*(v_i) + \Delta D_i(v_i)$, $(\cdot)_i^*$ represents the nominal part that can be determined by the computational fluid dynamics (CFD) [36]. $\Delta(\cdot)_i$ denotes the difference between the actual and nominal parts, i.e., model uncertainties.
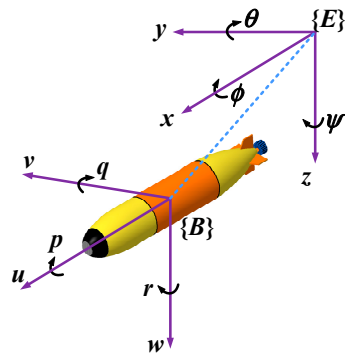
Figure 1. AUV coordinate system.

Then, the dynamic model (2) of ith AUV with the above constraints is rewritten as:

$$M_i^* \dot{v}_i + C_i^*(v_i)v_i + D_i^*(v_i)v_i = \tau_i + \tau_{id} \qquad (4)$$

where $\tau_{id} = \tau_{ic} - \Delta M_i \dot{v}_i - \Delta C_i(v_i)v_i - \Delta D_i(v_i)v_i$ is considered as the lumped disturbance, including environmental disturbances and model uncertainties. In general, external disturbances exhibit limited energy and periodic variations. The model uncertainties are limited by the actual state and physical features of the AUV. Therefore, we make the following rational assumption:

Assumption 1 ([37]). *The external disturbance τ_{ic} and its first derivative $\dot{\tau}_{ic}$ are bounded, and the model uncertainties ΔM_i, ΔC_i, and ΔD_i are unknown and bounded. Therefore, the lumped disturbance τ_{id} is bounded and satisfies $\|\tau_{id}\| \leq \overline{\tau}_{id}$, $\overline{\tau}_{id} \in \mathbb{R}^+$.*

3.2. Problem Formulation

To better characterize the information exchange between the AUVs, we adopted a directed topology graph $G = \{V, \varepsilon\}$ to describe the formation communication. The node set $V = \{V_1, V_2, \cdots, V_N\}$ denotes the N AUVs, and an edge set $\varepsilon \subseteq V \times V$ describes the information interaction from the node V_i to the node V_j. Define $A = [a_{ij}]$ as an adjacency matrix, where a_{ij} denotes the connection weight and $a_{ij} = 1$ if $(i, j) \in \varepsilon$, while $a_{ij} = 0$ if $(i, j) \notin \varepsilon$. Presume that the ith AUV has the capability to receive local information from the virtual leader and the neighbors $N_i = \{j \in V : (j, i) \in \varepsilon\}$ [38].

Next, we formulate the AUV formation tracking control problem. In order for the AUV formation to track the reference trajectory η_r smoothly while maintaining the prescribed shape, the ith AUV is driven to satisfy: (1) Tracking: $\lim_{t \to \infty} \|\eta_i(t) - \eta_r(t)\| = d_{ir}$; $\lim_{t \to \infty} \|v_i(t) - v_{id}(t)\| = 0$. (2) Formation: $\lim_{t \to \infty} \|\eta_i(t) - \eta_j(t)\| = d_{ij}$, with d_{ir} denoting the formation configuration vector and d_{ij} denoting the relative distance vector between the ith AUV and the jth AUV.

4. Methodology

In this section, to address the AUV formation control issue subject to complex constraints, we develop a novel distributed Lyapunov-based model predictive tracking control scheme. Initially, recognizing the presence of lumped disturbances that cannot be directly measured, a fast FTESO is devised to compensate for this constraint. Then, we make structural adaptation to the existing DLMPC method that uses a hierarchical design of position and velocity tracking controllers to handle the other constraints. Stability constraints are constructed based on Lyapunov theory. Finally, we analyze the feasibility and stability of the AUV formation system.

4.1. Design and Stability Analysis of FFTESO

Given the efficacy of the extended state observation method in estimating disturbances and model uncertainties, we propose a novel FFTESO to concurrently compensate for the lumped disturbances within the AUV formation.

To facilitate the FFTESO design, the AUV dynamics model (4) with respect to the earth-fixed frame can be further transformed as:

$$\ddot{\eta}_i = -M_{i\eta}^{-1}\Big[C_{i\eta}\dot{\eta}_i + D_{i\eta}\dot{\eta}_i - J_i^{-T}(\eta_i)(\tau_i + \tau_{id})\Big] \tag{5}$$

where $C_{i\eta} = J_i^{-T}(\eta_i)\Big[C_i^*(v_i) - M_i^*J_i^{-1}(\eta_i)\dot{J}_i(\eta_i)\Big]J_i^{-1}(\eta_i)$, $D_{i\eta} = J_i^{-T}(\eta_i)D_i^*(v_i)J_i^{-1}(\eta_i)$, $M_{i\eta} = J_i^{-T}(\eta_i)M_i^*J_i^{-1}(\eta_i)$. Then, define the auxiliary variables $\mu_i = \dot{\eta}_i = J_i(\eta_i)v_i$, $f_i(\mu_i)\mu_i = M_{i\eta}^{-1}(C_{i\eta} + D_{i\eta})\dot{\eta}_i$, $d_i = M_{i\eta}^{-1}J_i^{-T}(\eta_i)\tau_{id}$, so the AUV's system model (1) and (2) are transformed to

$$\begin{cases} \dot{\eta}_i = \mu_i \\ \dot{\mu}_i = -f_i(\mu_i)\mu_i + M_{i\eta}^{-1}J_i^{-T}\tau_i + d_i \end{cases} . \tag{6}$$

Next, we define some new variables $z_{i1} = \eta_i$, $z_{i2} = \mu_i$, and the lumped disturbances are regarded as an extended state z_{i3}, denoted as $z_{i3} = d_i$ with $\dot{z}_{i3} = \sigma_i$. In Assumption 1, d_i is bounded and continuously differentiable as well, and the components of its first derivative σ_i satisfies $|\sigma_{ip}| \leq \overline{\sigma}_i$, $p = 1, 2, \ldots, 5$, where $\overline{\sigma}_i$ is an unknown upper bound. Afterward, the mathematical model of the *i*th AUV can be extended as:

$$\begin{cases} \dot{z}_{i1} = z_{i2} \\ \dot{z}_{i2} = -f_i(z_{i2})z_{i2} + M_{i\eta}^{-1}J_i^{-T}\tau_i + z_{i3} \\ \dot{z}_{i3} = \sigma_i \end{cases} . \tag{7}$$

Denote $\hat{z}_{i1}$, $\hat{z}_{i2}$, and $\hat{z}_{i3}$ as the estimation of states z_{i1}, z_{i2} and z_{i3} in the extended system (7), and $e_{i1} = \hat{z}_{i1} - z_{i1}$, $e_{i2} = \hat{z}_{i2} - z_{i2}$, $e_{i3} = \hat{z}_{i3} - z_{i3}$ as the estimation errors of the position, velocity, and lumped disturbance, respectively. Then, the FFTESO for the *i*th AUV is designed as:

$$\begin{cases} \dot{\hat{z}}_{i1} = \hat{z}_{i2} - \beta_{i1}\big(\lceil e_{i1}\rfloor^{\alpha_{i1}} + e_{i1}\big) \\ \dot{\hat{z}}_{i2} = \hat{z}_{i3} - \beta_{i2}\big(\lceil e_{i1}\rfloor^{\alpha_{i2}} + \gamma_i e_{i1}\big) - f_i(\hat{z}_{i2})\hat{z}_{i2} + M_{i\eta}^{-1}J_i^{-T}\tau_i \\ \dot{\hat{z}}_{i3} = -\beta_{i3}\big(\lceil e_{i1}\rfloor^{\alpha_{i3}} + \gamma_i^2 e_{i1}\big) \end{cases} \tag{8}$$

with the observer gains satisfying $\beta_{ik} > 0$, $k = 1, 2, 3$, $\alpha_{i1} \in (2/3, 1)$ and $\alpha_{i2} = 2\alpha_{i1} - 1$, $\alpha_{i3} = 3\alpha_{i1} - 2$, $\gamma_i = |e_{i1}|^{\alpha_{i1}-1}$, $\lceil e_{i1}\rfloor^{\alpha_{ik}} = \text{sign}(e_{i1})|e_{i1}|^{\alpha_{ik}}$ with $|e_{i1}|^{\alpha_{ik}} = \big[|e_{i11}|^{\alpha_{ik}}, |e_{i12}|^{\alpha_{ik}}\big], \ldots,$ $\big[|e_{i1n}|^{\alpha_{ik}}\big]^T$. Based on the model (7) and the designed FFTESO (8), the observation error dynamics are:

$$\begin{cases} \dot{e}_{i1} = e_{i2} - \beta_{i1}\big(\lceil e_{i1}\rfloor^{\alpha_{i1}} + e_{i1}\big) \\ \dot{e}_{i2} = e_{i3} - \beta_{i2}\big(\lceil e_{i1}\rfloor^{\alpha_{i2}} + \gamma_i e_{i1}\big) + f_i(z_{i2})z_{i2} - f_i(\hat{z}_{i2})\hat{z}_{i2} \\ \dot{e}_{i3} = -\beta_{i3}\big(\lceil e_{i1}\rfloor^{\alpha_{i3}} + \gamma_i^2 e_{i1}\big) - \sigma_i \end{cases} . \tag{9}$$

The convergence analysis of the FFTESO (8) is presented in the following theorem.

Theorem 1. *Consider the formation control system of the AUV model (7) under Assumption 1. If the FFTESO is designed as in (8) to satisfy the specified observer gain constraints, then the estimation errors $e_i = \big[e_{i1}^T, e_{i2}^T, e_{i3}^T\big]^T$ will converge to the stability region Ω_i within a finite time T_{if}.*

Proof. See Appendix A. □

4.2. Position Tracking Controller

In this subsection, we explain our design of the DLMPC-based position tracking controller. It makes the ith AUV track the reference trajectory $\boldsymbol{\eta}_r$ by outputting the desired driving speed, thereby converging the position tracking error. It supplies the optimal desired speed needed by the velocity tracking controller.

The reference trajectory is defined as $\boldsymbol{\eta}_r = [x_r, y_r, z_r, \theta_r, \psi_r]^T$. Here, to avoid singularities in the reference trajectory, we make the following assumption:

Assumption 2 ([25]). *The reference trajectory $\boldsymbol{\eta}_r$ and its derivatives are smooth and bounded, satisfying the equation $\|\boldsymbol{\eta}_r\|_\infty \leq \overline{\eta}_r$, $\|\dot{\boldsymbol{\eta}}_r\|_\infty \leq \overline{\eta}_{r1}$, $\|\ddot{\boldsymbol{\eta}}_r\|_\infty \leq \overline{\eta}_{r2}$ with positive constants $\overline{\eta}_r$, $\overline{\eta}_{r1}$, $\overline{\eta}_{r2}$.*

The kinematic model for the ith AUV position tracking can be established by (1):

$$\dot{\boldsymbol{x}}_{i1} = \boldsymbol{J}_i(\boldsymbol{\eta}_i)\boldsymbol{v}_i = f_{i1}(\boldsymbol{x}_{i1}, \boldsymbol{u}_{i1}) \tag{10}$$

where $\boldsymbol{x}_{i1} = [x_i, y_i, z_i, \theta_i, \psi_i]^T$ and $\boldsymbol{u}_{i1} = [u_i, v_i, w_i, q_i, r_i]^T$ are the state and the control input of the ith AUV, respectively. To fulfill the control objective of each AUV, the DLMPC optimization problem for the position tracking controller can be formulated as:

$$\min_{\boldsymbol{u}_{i1} \in C(h)} J_{i1} = \int_0^T \left(\sum_{j \in \mathrm{N}_i} a_{ij} \|\boldsymbol{x}_{ij}(s)\|_{\boldsymbol{Q}_{ij}}^2 + \|\tilde{\boldsymbol{x}}_{i1}(s)\|_{\boldsymbol{Q}_{i1}}^2 + \|\boldsymbol{u}_{i1}(s)\|_{\boldsymbol{R}_{i1}}^2 \right) ds \tag{11a}$$

$$s.t. \ \dot{\widehat{\boldsymbol{x}}}_{i1}(s) = f_{i1}\left(\widehat{\boldsymbol{x}}_{i1}(s), \boldsymbol{u}_{i1}(s) \right) \tag{11b}$$

$$\widehat{\boldsymbol{x}}_{i1}(0) = \boldsymbol{x}_{i1}|_{t=t_0} \tag{11c}$$

$$x_{i1}^{\min} \leq \widehat{\boldsymbol{x}}_{i1}(s) \leq x_{i1}^{\max} \tag{11d}$$

$$\|\boldsymbol{u}_{i1}(s)\|_\infty \leq u_{i1}^{\max} \tag{11e}$$

$$\dot{V}_{ip}\Big|_{\boldsymbol{u}_{i1}(0)} \leq \dot{V}_{ip}\Big|_{\boldsymbol{u}_{i1}^{vir}(0)} \tag{11f}$$

where $\widehat{\boldsymbol{x}}_{i1}(s)$ denotes the predicted state trajectory, $\boldsymbol{x}_{ij} = \widehat{\boldsymbol{x}}_{i1} - \widehat{\boldsymbol{x}}_{j1} - d_{ij}$, $\tilde{\boldsymbol{x}}_{i1} = \widehat{\boldsymbol{x}}_{i1} - \boldsymbol{\eta}_r - d_{ir}$. $C(h)$ represents the cluster of piecewise functions featured by the sampling period h, $T = Mh$ denotes the prediction horizon. $\boldsymbol{Q}_{ij}$, $\boldsymbol{Q}_{i1}$ and $\boldsymbol{R}_{i1}$ represent weighting matrices that are diagonal and positive-definite. (11c) is the initial state condition. (11d) represents the position state constraint. (11e) represents the control input constraint. (11f) is the stability constraint constructed by the Lyapunov-based virtual control law $\boldsymbol{u}_{i1}^{vir}$ and the relevant Lyapunov function V_{ip}, which explicitly characterizes the guaranteed region of attraction. This is designed to circumvent the local linearization of the standard DMPC while guaranteeing the stability of the formation tracking. One should note that $\boldsymbol{u}_{i1}^{vir}$ does not actually control the vehicle but only ensures system stability.

Then, we construct the concrete expression of the stability constraints in (11f), which involves determining an appropriate state-feedback controller and the corresponding Lyapunov function. Various nonlinear control techniques, such as sliding mode control and backstepping, can be employed. For the trajectory tracking problem, we select the backstepping method to develop the Lyapunov-based nonlinear controller.

Let $\boldsymbol{\eta}_i$ denote the trajectory of the ith AUV, and $\boldsymbol{\eta}_{ir} = \boldsymbol{\eta}_r + \boldsymbol{d}_{ir} = [x_{ir}, y_{ir}, z_{ir}, \theta_{ir}, \psi_{ir}]^T$ be the desired path; $\tilde{\boldsymbol{\eta}}_i = \boldsymbol{\eta}_i - \boldsymbol{\eta}_{ir}$ represents the position tracking error of ith AUV. Define the following Lyapunov function:

$$V_{ip} = \frac{1}{2}\tilde{\boldsymbol{\eta}}_i^T \boldsymbol{\Lambda}_{i1}\tilde{\boldsymbol{\eta}}_i \tag{12}$$

where $\boldsymbol{\Lambda}_{i1} > 0$ is a specified control gain matrix, diagonal and positive-definite. Taking the time derivative of V_{ip}, we can obtain:

$$\dot{V}_{ip} = \tilde{\boldsymbol{\eta}}_i^{-T} \boldsymbol{\Lambda}_{i1} \dot{\tilde{\boldsymbol{\eta}}}_i = \tilde{\boldsymbol{\eta}}_i^{-T} \boldsymbol{\Lambda}_{i1} (J_i(\boldsymbol{\eta}_i)\boldsymbol{v}_i - \dot{\boldsymbol{\eta}}_r). \tag{13}$$

To stabilize the position tracking, we choose the following control law:

$$\boldsymbol{v}_i^{vir} = J_i^{-1}(\boldsymbol{\eta}_i)\left(\dot{\boldsymbol{\eta}}_r - \boldsymbol{K}_{ip}\tilde{\boldsymbol{\eta}}_i\right) \tag{14}$$

where $\boldsymbol{K}_{ip} > 0$ is another specified control gain matrix. Then, the derivative of V_{ip} (13) becomes the following form:

$$\dot{V}_{ip} = -\tilde{\boldsymbol{\eta}}_i^{-T} \boldsymbol{\Lambda}_{i1} \boldsymbol{K}_{ip}\tilde{\boldsymbol{\eta}}_i. \tag{15}$$

From (12) and (15), it can be seen that $V_{ip} > 0$ and $\dot{V}_{ip} \leq 0$, so based on Lyapunov's direct method, the position tracking subsystem with virtual control law (14) is globally asymptotically stable with respect to the equilibrium $\left[\tilde{\boldsymbol{\eta}}_i, \ \boldsymbol{v}_i\right] = [0, \ 0]$. Therefore, we can obtain the concrete expression of the stability constraint (11f) as follows:

$$\tilde{\boldsymbol{\eta}}_i^{-T}(0)\boldsymbol{\Lambda}_{i1}\big(J_i(\boldsymbol{\eta}_i(0))\boldsymbol{v}_i(0) - \dot{\boldsymbol{\eta}}_r(0)\big) \leq -\tilde{\boldsymbol{\eta}}_i^{-T}(0)\boldsymbol{\Lambda}_{i1}\boldsymbol{K}_{ip}\tilde{\boldsymbol{\eta}}_i(0). \tag{16}$$

The stability constraint (16) facilitates the verification that the DLMPC inherits the stability properties of the state-feedback control law (14) [39]. Moreover, owing to the online optimization process, the DLMPC-based position controller will automatically execute the optimal control performance obeying the system constraints.

4.3. Velocity Tracking Controller

In this subsection, we design a DLMPC-based velocity tracking controller to obtain the optimal control forces and moments of the ith AUV, aiming to track the desired velocity. It is used to stabilize the velocity tracking error in the AUV dynamics subsystem.

The dynamic model for the ith AUV velocity tracking can be modeled by (4):

$$\dot{\boldsymbol{x}}_{i2} = \boldsymbol{M}_i^{*-1}(\boldsymbol{\tau}_i + \boldsymbol{\tau}_{id} - \boldsymbol{C}_i^*(\boldsymbol{v}_i)\boldsymbol{v}_i - \boldsymbol{D}_i^*(\boldsymbol{v}_i)\boldsymbol{v}_i) = f_{i2}(\boldsymbol{x}_{i2}, \ \boldsymbol{u}_{i2}, \ \boldsymbol{\tau}_{id}) \tag{17}$$

where the state is defined as $\boldsymbol{x}_{i2} = [u_i, v_i, w_i, q_i, r_i]^T$ and the control input is defined as $\boldsymbol{u}_{i2} = [\tau_{iu}, \tau_{iv}, \tau_{iw}, \tau_{iq}, \tau_{ir}]^T$. Based on the effect of FFTESO (8) and the control objective, the DLMPC optimization problem for the velocity tracking controller can be formulated as:

$$\min_{\boldsymbol{u}_{i2}\in C(h)} J_{i2} = \int_0^T \left(\left\|\tilde{\boldsymbol{x}}_{i2}(s)\right\|_{\boldsymbol{Q}_{i2}}^2 + \|\boldsymbol{u}_{i2}(s)\|_{\boldsymbol{R}_{i2}}^2\right)ds \tag{18a}$$

$$s.t. \ \dot{\widehat{\boldsymbol{x}}}_{i2}(s) = f_{i2}\left(\widehat{\boldsymbol{x}}_{i2}(s), \ \boldsymbol{u}_{i2}(s), \ \widehat{\boldsymbol{\tau}}_{id}(s)\right) \tag{18b}$$

$$\widehat{\boldsymbol{x}}_{i2}(0) = \boldsymbol{x}_{i2}|_{t=t_0} \tag{18c}$$

$$x_{i2}^{\min} \leq \widehat{\boldsymbol{x}}_{i2}(s) \leq x_{i2}^{\max} \tag{18d}$$

$$\|\boldsymbol{u}_{i2}(s)\|_\infty \leq u_{i2}^{\max} \tag{18e}$$

$$\dot{V}_{iv}\Big|_{\boldsymbol{u}_{i2}(0)} \leq \dot{V}_{iv}\Big|_{\widehat{\boldsymbol{u}}_{i2}^{vir}(0)} \tag{18f}$$

where $\widehat{\boldsymbol{x}}_{i2}(s)$ is the predicted state trajectory, and $\tilde{\boldsymbol{x}}_{i2} = \widehat{\boldsymbol{x}}_{i2} - v_{id}$ denotes the tracking error. The desired speed v_{id} is derived from the position tracking controller (11). $\boldsymbol{Q}_{i2}$ and $\boldsymbol{R}_{i2}$ rep-

resent positive-definite weighting matrices. Similar to the optimization problem (11), the condition (18c) denotes the initial state. (18d) represents the velocity state constraint. (18e) represents the control input constraint. (18f) is the stability constraint constructed by the virtual control law $\hat{u}_{i2}^{vir}$ and the corresponding Lyapunov function V_{iv}. The DLMPC controller (18) inherits the stability and robustness of the virtual controller. Then, we construct the concrete expression of the stability constraints.

Let v_i denote the velocity of the *i*th AUV, where $\tilde{v}_i = v_i - v_{id}$ represents the velocity tracking error of *i*th AUV. Consider the following Lyapunov function:

$$V_{iv} = \frac{1}{2}\tilde{v}_i^T \Lambda_{i2}\tilde{v}_i + V_{ip} \tag{19}$$

where $\Lambda_{i2} > 0$ is a positive-definite diagonal matrix. Taking the time derivative of V_{iv}, we can derive:

$$\dot{V}_{iv} = \tilde{v}_i^T \Lambda_{i2}\dot{\tilde{v}}_i + \dot{V}_{ip} = \tilde{v}_i^T \Lambda_{i2}\left[M_i^{*-1}(\tau_i + \tau_{id} - C_i^*(v_i)v_i - D_i^*(v_i)v_i) - \dot{v}_{id} \right] - \tilde{\eta}_i^T \Lambda_{i1}K_{ip}\tilde{\eta}_i. \tag{20}$$

To achieve stable velocity tracking, based on the backstepping method and the lumped disturbances compensated by FFTESO, we choose the following control law:

$$\tau_i^{vir} = C_i^*(v_i)v_i + D_i^*(v_i)v_i + M_i^*\dot{v}_{id} - M_i^*K_{iv}\tilde{v}_i - \hat{\tau}_{id} \tag{21}$$

where $K_{iv} > 0$ is a specified gain matrix. Then, (13) becomes the following form:

$$\dot{V}_{iv} = -\tilde{v}_i^T \Lambda_{i2}K_{iv}\tilde{v}_i - \tilde{\eta}_i^T \Lambda_{i1}K_{ip}\tilde{\eta}_i. \tag{22}$$

From (19) and (22), it can be seen that $V_{iv} > 0$ and $\dot{V}_{iv} \leq 0$, so according to Lyapunov's direct method, the velocity tracking subsystem with virtual control law (21) is globally asymptotically stable with respect to the equilibrium $\left[\tilde{v}_i, \tau_i\right] = [0, 0]$. Thus, the concrete expression of the stability constraint (18f) is:

$$\begin{aligned} \tilde{v}_i^T(0)\Lambda_{i2}&\left[M_i^{*-1}\left(\tau_i(0) + \hat{\tau}_{id}(0) - C_i^*(v_i(0))v_i(0) - D_i^*(v_i(0))v_i(0) \right) - \dot{v}_{id}(0) \right] \\ &\leq -\tilde{v}_i^T(0)\Lambda_{i2}K_{iv}\tilde{v}_i(0). \end{aligned} \tag{23}$$

Likewise, the DLMPC-based velocity controller exerts excellent control performance thanks to online optimization. Leveraging the designed position controller (11) and velocity controller (18), the distributed Lyapunov-based model predictive formation control will be implemented for each AUV in the receding horizon mode.

The implementation process of DLMPC is described in Algorithm 1. The core of the algorithm consists of two parts: solving the optimization problem (11) of the position tracking layer and solving the optimization problem (18) of the velocity tracking layer. Firstly, the optimization problem (11) is solved, yielding the optimal control input related to AUV linear and angular velocity variables. Then, the control inputs of the position tracking layer are passed as reference velocity to the velocity tracking layer. By solving the optimization problem (18), the optimal control force and torque are obtained. Finally, the control inputs of the velocity tracking layer are applied to the AUV system. Figure 2 shows the flow diagram of the proposed Algorithm 1.

Algorithm 1. DLMPC Implementation

1: The *i*th AUV samples the current state $\boldsymbol{\eta}_i(t)$. Input the cost function J_{i1} in (11a).

2: The *i*th AUV receives the state trajectory of its neighbor AUV $\widehat{\boldsymbol{x}}_{j1}(t)$, $j \in V$, $j \neq i$.

3: Solve the optimization problem (11) provided $\boldsymbol{x}_{i1}|_{t=t_0} = \boldsymbol{\eta}_i(t)$, generate $\boldsymbol{\kappa}_{i1}(s)$, and let it be the (sub-)optimal solution.

4: Implement $\boldsymbol{\kappa}_{i1}(s)$ for only one sampling period, i.e., $\boldsymbol{u}_{i1}(t) = \boldsymbol{\kappa}_{i1}(s)$ for $s \in [0, h]$.

5: Let $\boldsymbol{v}_{id}(t) = \boldsymbol{u}_{i1}(t)$, input the cost function J_{i2} in (18a).

6: Solve the optimization problem (18) provided, $\boldsymbol{x}_{i2}|_{t=t_0} = \boldsymbol{v}_i(t)$, generating $\boldsymbol{\kappa}_{i2}(s)$.

7: Implement $\boldsymbol{\kappa}_{i2}(s)$ for only one sampling period, i.e., $\boldsymbol{u}_{i2}(t) = \boldsymbol{\kappa}_{i2}(s)$ for $s \in [0, h]$.

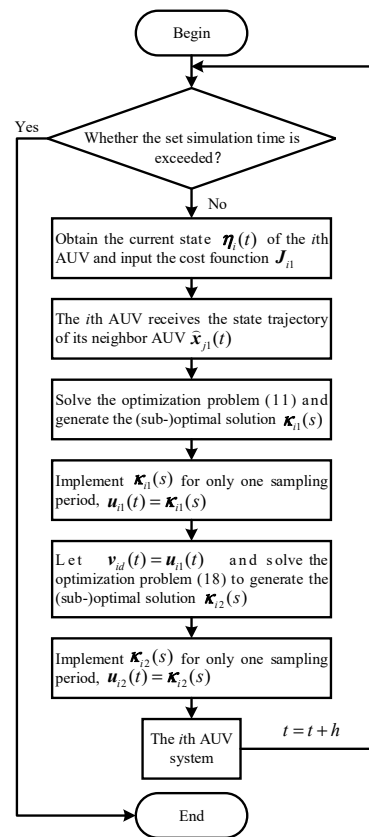8: At next sampling time instant, set $t = t + h$, and repeat from step 1.

Figure 2. Flow diagram of Algorithm 1.

Remark 1. *In the next section, we demonstrate that both system stability and recursive feasibility are not dependent on obtaining the precise solution from the optimization process. Therefore, suboptimal solutions are deemed acceptable in Algorithm 1. The use of iterative methods ensures that DLMPC optimization problems (11) and (18) possess locally optimal solutions. We can trade off numerical efficacy and control effect by setting the maximum iteration number without compromising the stability of the formation control. Additionally, the compensation of lumped disturbances is continuously applied throughout the iterative optimization process, ensuring the success of the formation tracking task under multiple constraints.*

4.4. Stability Analysis

In the previous subsection, stability constraints were constructed using the Lyapunov-based backstepping method. In this subsection, we will analyze the recursive feasibility and closed-loop stability of Algorithm 1.

First, we give the following theorem to show the recursive feasibility of the designed position tracking controller.

Theorem 2. *Choose the positive-definite gain matrix as $K_{ip} = \text{diag}\{k_{ip1}, k_{ip2}, k_{ip3}, k_{ip4}, k_{ip5}\}$. Let $\overline{K}_{ip}$ denote the largest entity in the control gain K_{ip}. For $u_{i1}^{vir}(x_{i1}) = v_i^{vir}(x_{i1})$, under Assumption 2, if the following relation can be ensured*

$$\left(1 + \frac{\sqrt{2}}{2}\right)\left(\overline{\eta}_{r1} + \overline{K}_{ip}\|\tilde{\eta}_i(0)\|\right) \leq v_i^{\max} \tag{24}$$

where $v_i^{\max} = \|v_i^{\max}\|_\infty$ denotes the maximum generalized velocity, then the DLMPC-based position controller is recursively feasible, i.e., $\left\|u_{i1}^{vir}\left(\hat{x}_{i1}(t)\right)\right\|_\infty \leq u_{i1}^{\max}$, for all $t \geq 0$.

Proof. See Appendix B. □

Then, we give the following theorem to show the recursive feasibility of the velocity controller.

Theorem 3. *Choose the positive definite gain matrix as $K_{iv} = \text{diag}\{k_{iv1}, k_{iv2}, k_{iv3}, k_{iv4}, k_{iv5}\}$. Let $\overline{K}_{iv}$ denote the largest entity in the control gain K_{iv}. For $\hat{u}_{i2}^{vir}(x_{i2}) = \tau_i^{vir}(x_{i2})$, under Assumption 1 and Assumption 2, if the following relation can be ensured*

$$\left(\overline{c}_i + \overline{d}_i\right)\overline{v}_i + \overline{m}_i\overline{v}_{id} + \left[\overline{K}_{iv} + \left(1 + \frac{\sqrt{2}}{2}\right)\right]\overline{m}_i\|\gamma_i(0)\| + \overline{\tau}_{id} \leq \tau_i^{\max} \tag{25}$$

where $\overline{v}_i = \left(1 + \frac{\sqrt{2}}{2}\right)\left(\overline{\eta}_{r1} + \overline{K}_{ip}\|\gamma_i(0)\|\right)$, $\overline{v}_{id} = \frac{2+\sqrt{2}}{h}\left(\overline{\eta}_{r1} + \overline{K}_{ip}\|\gamma_i(0)\|\right)$, $\tau_i^{\max}$ is the maximum possible generalized thrust force, $\overline{m}_i$ is a known constant bound for M_i^*. Then, the velocity controller is recursively feasible, i.e., $\left\|\hat{u}_{i2}^{vir}\left(\hat{x}_{i2}(t)\right)\right\|_\infty \leq u_{i2}^{\max}$, for all $t \geq 0$.

Proof. See Appendix C. □

Finally, we give the following theorem to show the stability of closed-loop system.

Theorem 4. *Consider the AUV formation control system described by (10) and (17) with lumped disturbances. If Assumption 1 and Assumption 2 hold, then the DLMPC-based position controller (11) renders the equilibrium $\left[\tilde{\eta}_i, \ v_i\right] = [0, \ 0]$ asymptotically stable, and the velocity controller (18) renders the equilibrium $\left[\tilde{v}_i, \ \tau_i\right] = [0, \ 0]$ asymptotically stable. In other words, the AUV formation tracking task can be realized under the control inputs produced by Algorithm 1.*

Proof. See Appendix D. □

5. Simulation

In this section, we conduct some simulation analyses to verify the effectiveness of the proposed hierarchical DLMPC algorithm for the AUV formation system. The formation network comprises four AUVs ($N = 4$, $i = 1, 2, 3, 4$) and a virtual leader (AUV0). Figure 3 illustrates the adopted communication topology, with the arrows indicating the communication direction between the AUVs. The simulation results demonstrate the promising formation tracking performance and robustness of the proposed method.
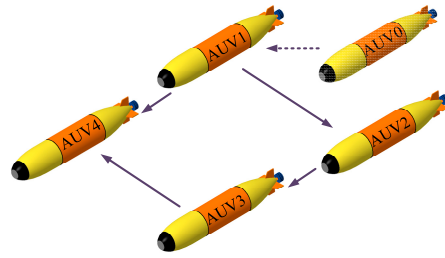
Figure 3. Structure of communication topology.

5.1. Simulation Setup

The initial states for each AUV are selected as $\boldsymbol{\eta}_1 = [17m, 28m, -2m, 0.08rad, 2rad]^T$, $\boldsymbol{\eta}_2 = [21m, 23m, -8m, 0.06rad, 2rad]^T$, $\boldsymbol{\eta}_3 = [20m, 8m, -6m, -0.05rad, 2.3rad]^T$ and $\boldsymbol{\eta}_4 = [30m, 17m, -3m, -0.06rad, 2.6rad]^T$, respectively. The model parameters for the homogeneous AUV were extracted from previous work [40]. We selected a diamond-shaped formation conducive to omnidirectional marine exploration, setting the formation configuration vectors as $\boldsymbol{d}_{1r} = [0, 0, 8, 0, 0]^T$, $\boldsymbol{d}_{2r} = [0, -6, 0, 0, 0]^T$, $\boldsymbol{d}_{3r} = [0, 0, -8, 0, 0]^T$, $\boldsymbol{d}_{4r} = [0, 6, 0, 0, 0]^T$. $\boldsymbol{d}_{12} = -\boldsymbol{d}_{21} = [0, 6, 8, 0, 0]^T$, $\boldsymbol{d}_{13} = -\boldsymbol{d}_{31} = [0, 0, 16, 0, 0]^T$, $\boldsymbol{d}_{14} = -\boldsymbol{d}_{41} = [0, -6, 8, 0, 0]^T$, $\boldsymbol{d}_{23} = -\boldsymbol{d}_{32} = [0, -6, 8, 0, 0]^T$, $\boldsymbol{d}_{24} = -\boldsymbol{d}_{42} = [0, -12, 0, 0, 0]^T$ and $\boldsymbol{d}_{34} = -\boldsymbol{d}_{43} = [0, -6, -8, 0, 0]^T$. The model uncertainties are reflected by considering 15% of the nominal value as the model error, implying that the AUV parameters in the simulation characterize only 85% of the nominal system. To assess the system's robustness, the external disturbances are modeled as follows:

$$\begin{cases} \tau_{icu} = 0.2\text{sign}(u_i) + 0.3\sin(t/10) \ N \\ \tau_{icv} = 0.1\text{sign}(v_i) + 0.2\sin(t/20) \ N \\ \tau_{icw} = 0.05\text{sign}(w_i) + 0.1\sin(t/5) \ N \\ \tau_{icq} = 0.2\text{sign}(q_i) + 0.1\sin(t/10) \ N \cdot m \\ \tau_{icr} = 0.3\text{sign}(r_i) + 0.2\sin(t/10) \ N \cdot m \end{cases} \quad (26)$$

There are guidelines for selecting each parameter: considering that AUVs navigate at slower speeds, a smaller T is planned to be adopted. During debugging, if the rate is not fast enough, adjust it down, and if the stability is poor, adjust it up. As we place more attention on the position tracking performance, $\boldsymbol{Q}_{i1}$ is set as slightly bigger than $\boldsymbol{Q}_{i2}$; to attenuate the interaction between angles, the angle weights in $\boldsymbol{Q}_{ij}$ are set a little smaller; $\boldsymbol{R}_{i1}$ and $\boldsymbol{R}_{i2}$ are set as small as possible while ensuring the stability of the system. The connection among the observer gains β_{ik} and α_{i1} is obtained by solving the Lyapunov equation (29), and then tuned to select appropriate values. Following the above guidelines, the simulation parameters of the proposed algorithm in Table 2 were chosen.

Table 2. Control parameters of the designed algorithm.

Parameter	Value	Parameter	Value
$\boldsymbol{Q}_{i1}$	$\text{diag}(10^3, 10^3, 10^3, 10^2, 10^2)$	h	0.1 s
$\boldsymbol{Q}_{ij}$	$\text{diag}(10^3, 10^3, 10^3, 10, 10)$	α_{i1}	0.75
$\boldsymbol{Q}_{i2}$	$\text{diag}(10^2, 10^2, 10^2, 10, 10)$	β_{i1}	0.8
$\boldsymbol{R}_{i1}$	$\text{diag}(10^{-2}, 10^{-2}, 10^{-2}, 10^{-2}, 10^{-2})$	β_{i2}	0.7
$\boldsymbol{R}_{i2}$	$\text{diag}(10^{-1}, 10^{-1}, 10^{-1}, 10^{-1}, 10^{-1})$	β_{i3}	0.2
$\boldsymbol{K}_{ip}$	$\text{diag}(5, 5, 5, 1, 1)$	$\boldsymbol{\Lambda}_{i1}$	$\text{diag}(1, 1, 1, 1, 1)$
$\boldsymbol{K}_{iv}$	$\text{diag}(3, 3, 3, 1, 1)$	$\boldsymbol{\Lambda}_{i2}$	$\text{diag}(1, 1, 1, 1, 1)$

Moreover, the prediction horizon is $T = 10$ h, and the limitation of each actuator is 500 N. The upper and lower bound of velocity states are set as ± 2 m/s, ± 1.2 m/s, ± 0.7

m/s, ± 0.1 rad/s, ± 0.3 rad/s. The reference trajectory generated by a virtual leader is a helical curve:

$$\begin{cases} x_r(t) = 35\cos(\pi t/200) \\ y_r(t) = 35\sin(\pi t/200) \\ z_r(t) = -0.06t - 6 \end{cases} \tag{27}$$

5.2. Performance Tests for Lumped Disturbances Estimation

Firstly, to assess the disturbance rejection capability of the formation system under spatial disturbance constraints, we conducted comparative tests with the conventional FTESO in [19], the improved third-order FTESO in [31], and the designed FFTESO (8). Figure 4 illustrates the disturbance estimation error norms $\|e_{i3}\| = \|\hat{d}_i - d_i\|$ for each AUV under different observers. It is evident from the figure that the conventional FTESO exhibits slow convergence time and slight chattering. While the third-order FTESO achieves finite-time stabilization, it starts with a large initial error and displays slow convergence speed. In contrast, the proposed FFTESO not only ensures the convergence of the estimation error to a small neighborhood of the origin within a finite time but also outperforms the other two observers in terms of dynamic response speed and estimation accuracy. Therefore, owing to the advantages of fast transient response and high accuracy of the designed FFTESO (8), each AUV can more swiftly and accurately compensate for both external disturbances and internal uncertainties. This markedly fortifies the active disturbance rejection capability of the formation control system.
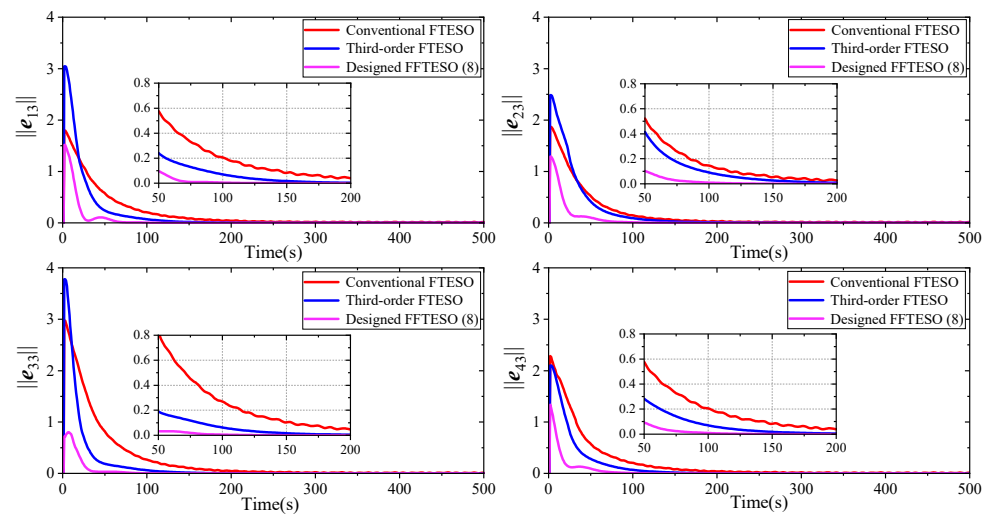

Figure 4. The estimation error norm $\|e_{i3}\|$ for the lumped disturbance of the *i*th AUV.

5.3. Performance Tests for Formation Trajectory Tracking

To evaluate the tracking control performance of the designed scheme, comparative tests were conducted under uniform parameter and disturbance settings: scheme (a) corresponds to our proposed FFTESO-based hierarchical DLMPC algorithm; scheme (b) corresponds to the conventional DLMPC algorithm for AUV formation in [30]; and scheme (c) corresponds to the ASTASMC algorithm proposed for AUV formation control in [23]. In the following section, we analyze the performance metrics of formation tracking control: convergence speed, tracking accuracy, and smoothness of control inputs.

Figures 5–9 depict the trajectories of the position and attitude angles of each AUV during formation tracking under both schemes. Figures 10–14 depict the trajectories of linear and angular velocities. Observing the results, it is evident that the three schemes successfully guided the four AUVs to the desired state. However, the tracking performance differed. In terms of convergence speed, scheme (a) achieved full-state stable tracking within 150 s, scheme (b) required 220 s, while in scheme (c) the entire process convergence took

about 300 s. In terms of tracking accuracy, unlike the observers used in (a) and (b), scheme (c) compensated for lumped disturbances through a robust adaptive law designed to mitigate high-frequency measurement noise. However, from the state trajectories, it is discernible that the state variables in (c) exhibited longer stabilization times and were accompanied by chattering. This indicates a weaker disturbance rejection capability compared to our proposed scheme. Furthermore, the comparison of (a) and (b) shows that the hierarchical structure enhances the rate of convergence and the controllability of the velocity state. The simulation results affirm that combining disturbance compensation from FFTESO and the online optimization of DLMPC strongly enhanced the formation control performance.
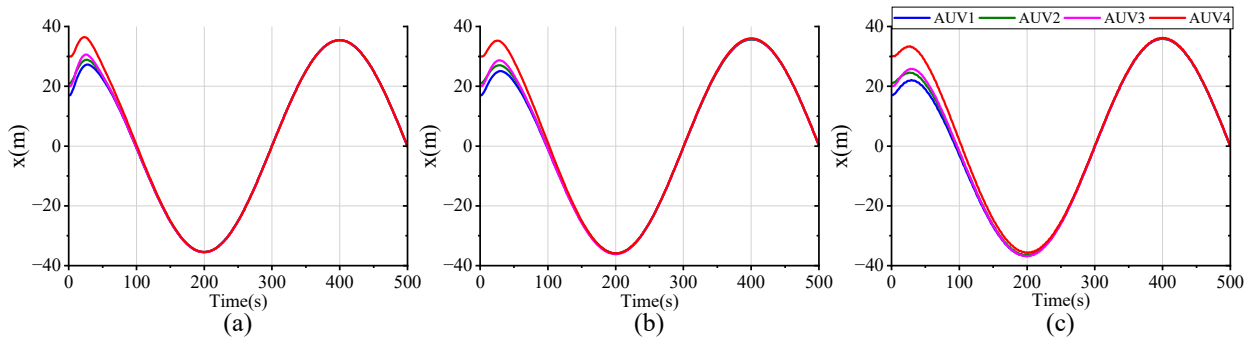
Figure 5. State x_i trajectories for multi-AUV systems. (**a**) The proposed hierarchical DLMPC scheme. (**b**) The conventional DLMPC scheme. (**c**) The ASTASMC scheme.
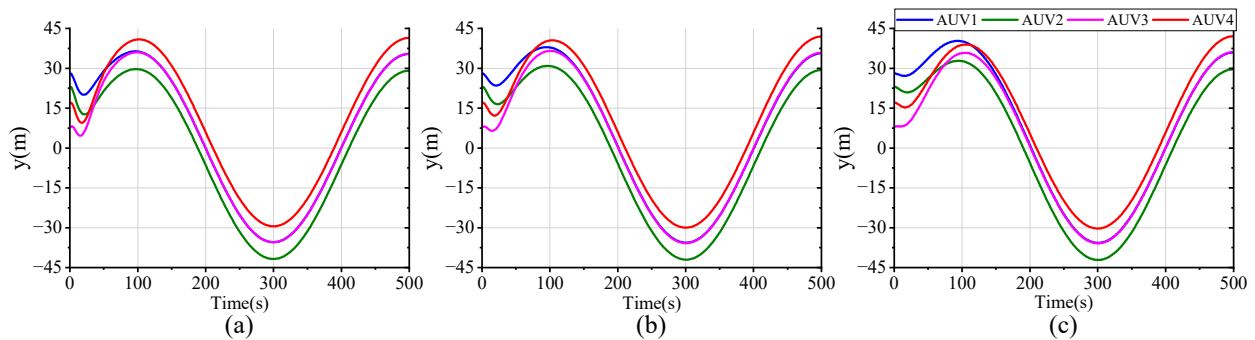
Figure 6. State y_i trajectories for multi-AUV systems. (**a**) The proposed hierarchical DLMPC scheme. (**b**) The conventional DLMPC scheme. (**c**) The ASTASMC scheme.
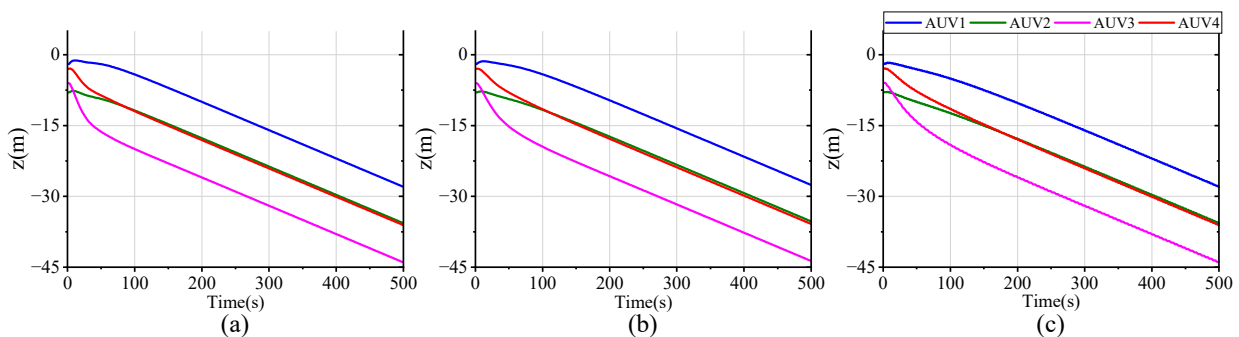
Figure 7. State z_i trajectories for multi-AUV systems. (**a**) The proposed hierarchical DLMPC scheme. (**b**) The conventional DLMPC scheme. (**c**) The ASTASMC scheme.

Figure 8. State θ_i trajectories for multi-AUV systems. (**a**) The proposed hierarchical DLMPC scheme. (**b**) The conventional DLMPC scheme. (**c**) The ASTASMC scheme.

Figure 9. State ψ_i trajectories for multi-AUV systems. (**a**) The proposed hierarchical DLMPC scheme. (**b**) The conventional DLMPC scheme. (**c**) The ASTASMC scheme.
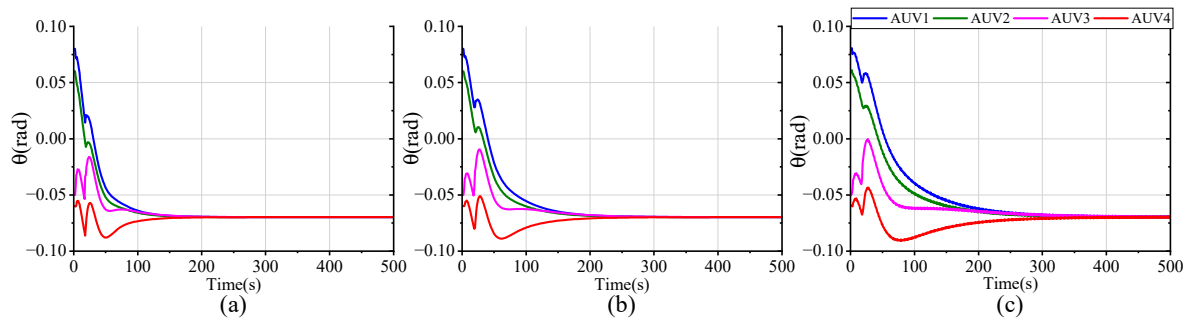

Figure 10. State u_i trajectories for multi-AUV systems. (**a**) The proposed hierarchical DLMPC scheme. (**b**) The conventional DLMPC scheme. (**c**) The ASTASMC scheme.
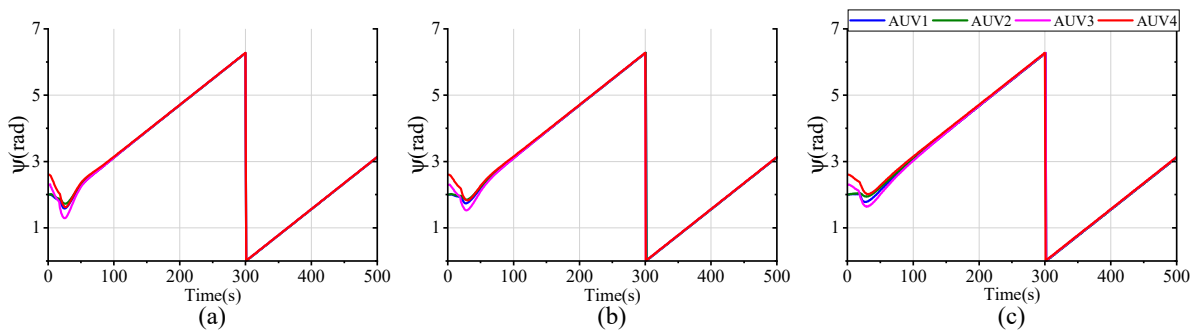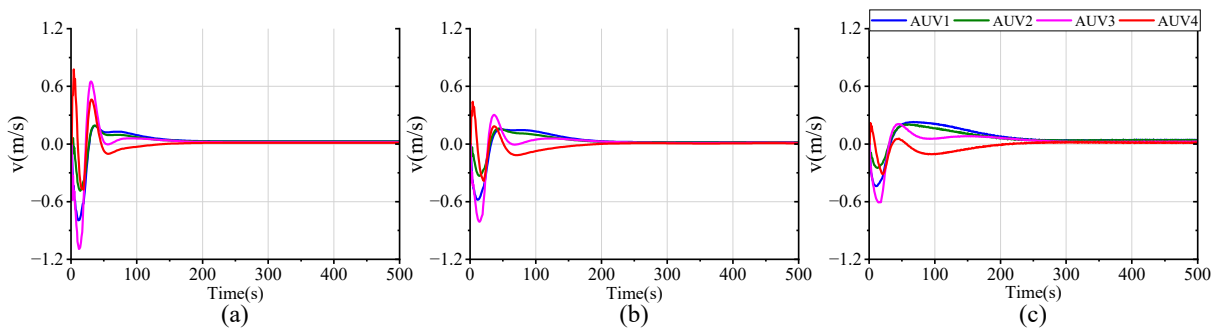

Figure 11. State v_i trajectories for multi-AUV systems. (**a**) The proposed hierarchical DLMPC scheme. (**b**) The conventional DLMPC scheme. (**c**) The ASTASMC scheme.

Figure 12. State w_i trajectories for multi-AUV systems. (**a**) The proposed hierarchical DLMPC scheme. (**b**) The conventional DLMPC scheme. (**c**) The ASTASMC scheme.
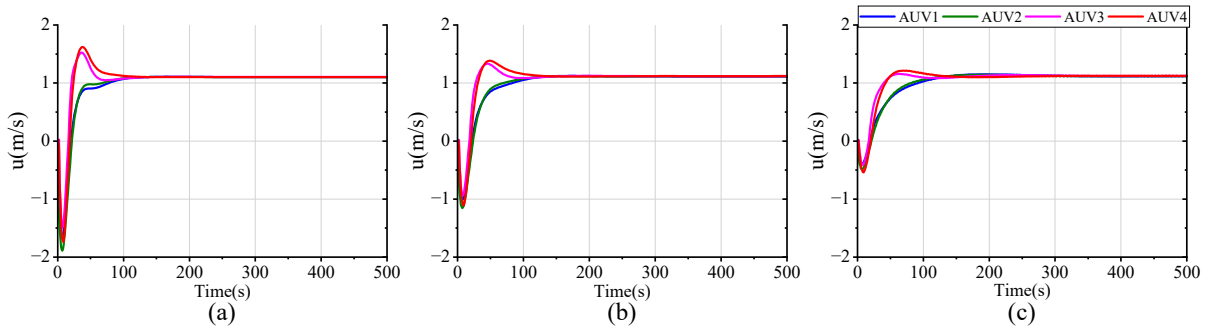

Figure 13. State q_i trajectories for multi-AUV systems. (**a**) The proposed hierarchical DLMPC scheme. (**b**) The conventional DLMPC scheme. (**c**) The ASTASMC scheme.

Figure 14. State r_i trajectories for multi-AUV systems. (**a**) The proposed hierarchical DLMPC scheme. (**b**) The conventional DLMPC scheme. (**c**) The ASTASMC scheme.
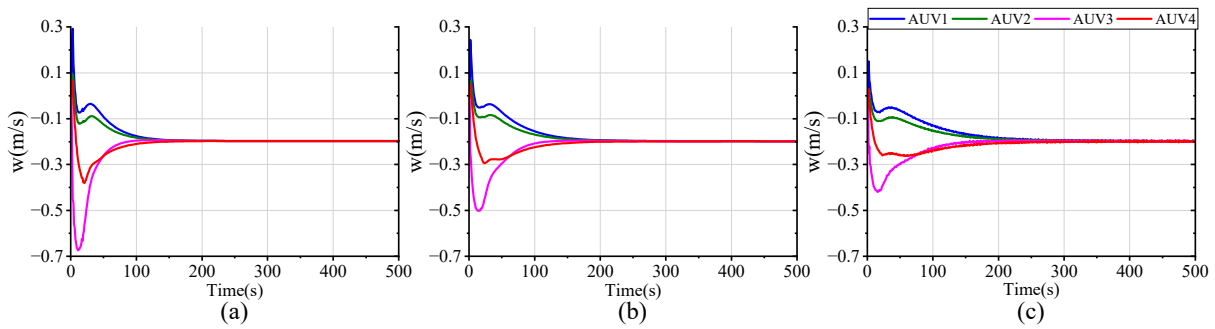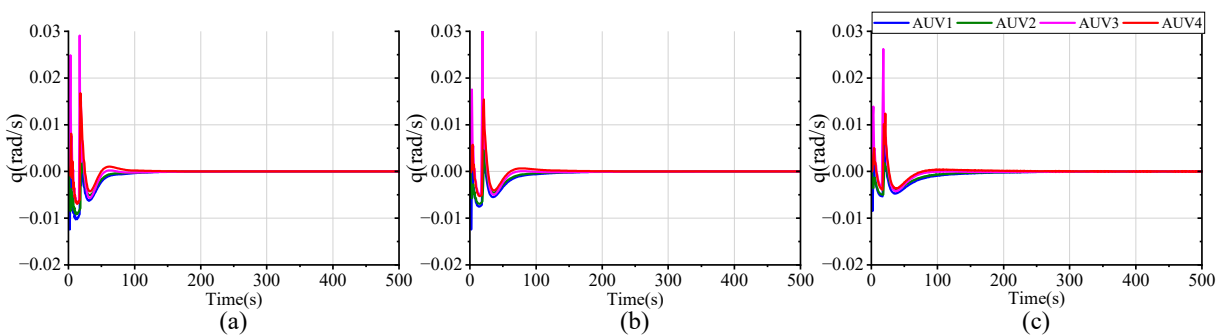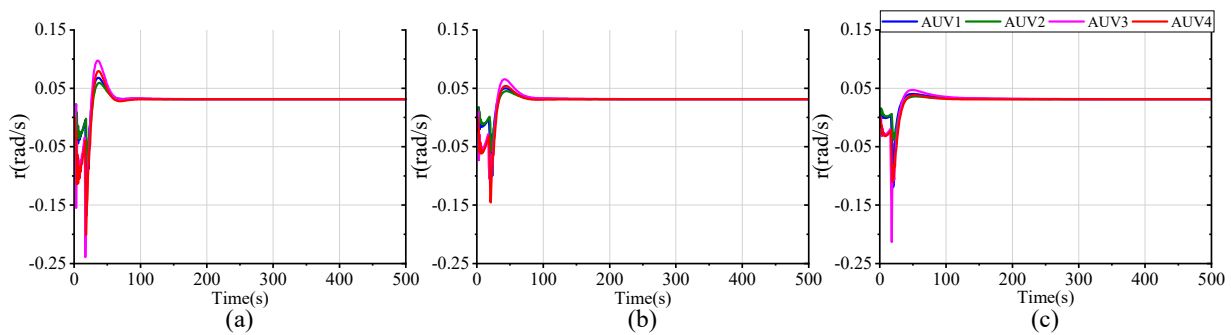
Figure 15 visually illustrates the formation tracking trajectory in three-dimensional space. In conjunction with Figures 5–14, it is evident that under the same initial conditions, all three schemes performed the formation helical dive task. However, scheme (c) was characterized by continuous fluctuations during the tracking process, posing an increased risk of the AUV formation deviating from the desired trajectory. Conversely, the formation members in schemes (a) and (b) smoothly tracked the reference trajectory while maintaining the preset distance. This difference arose from the distinct compensation principles of the disturbance rejection methods. The robust adaptive law in scheme (c) proved less robust to lumped disturbances with fast time-varying characteristics. On further observation, the proposed control scheme facilitated each AUV in forming the predefined configuration more rapidly, showcasing the superior response speed of the designed control system. Consequently, under multiple constraints such as lumped disturbances, state constraints, and stability constraints, the FFTESO-based DLMPC algorithm

exhibited greater adaptability to complex underwater environments than the other two algorithms in terms of disturbance rejection, convergence speed, and tracking performance. Figure 16 gives the tracking error for each AUV under the three schemes. Table 3 presents the convergence time of all states and the average of AUV3's tracking error after 130 s for the three schemes. We can clearly conclude that the proposed method had the optimal convergence speed and tracking accuracy.
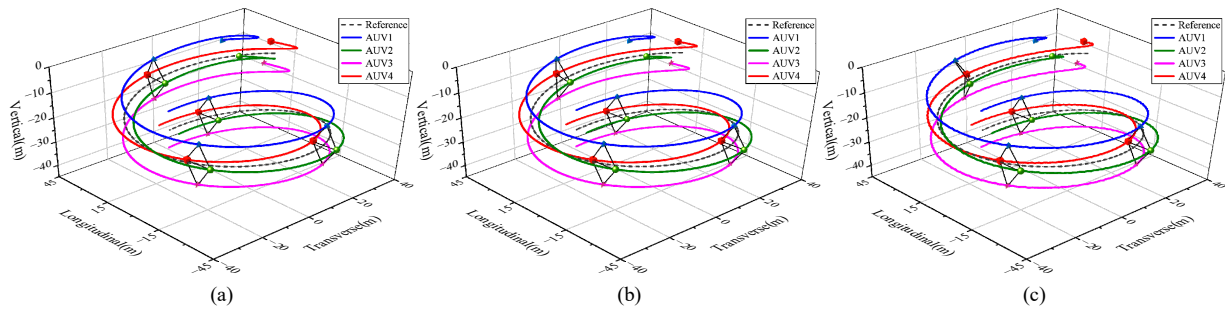

Figure 15. Three-dimensional trajectories of the multi-AUV systems under three schemes. (**a**) The designed hierarchical DLMPC scheme. (**b**) The conventional DLMPC scheme. (**c**) The ASTASMC scheme.
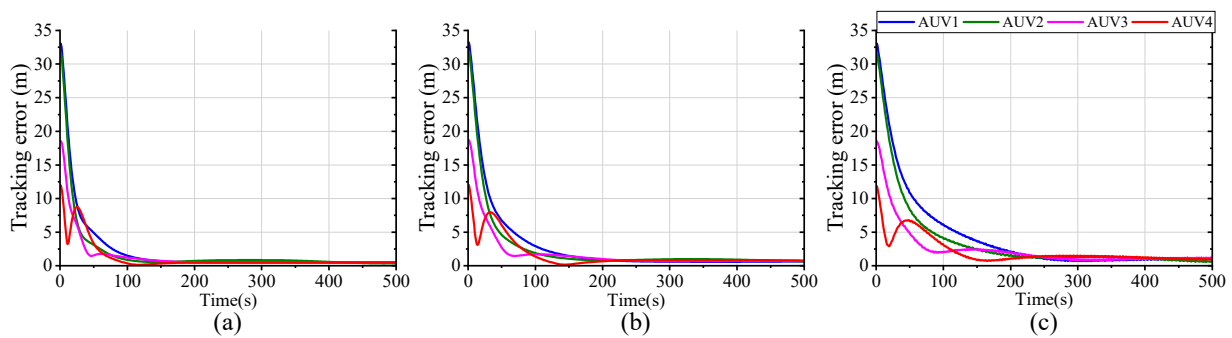

Figure 16. Tracking errors of the multi-AUV under three schemes. (**a**) The proposed hierarchical DLMPC scheme. (**b**) The conventional DLMPC scheme. (**c**) The ASTASMC scheme.

Table 3. Comparison of performance metrics.

Control Scheme	Convergence Time	Tracking Error Averages
Scheme (a)	150 s	0.508 m
Scheme (b)	220 s	0.830 m
Scheme (c)	300 s	1.341 m

Without loss of generality, Figure 17 illustrates the actual control forces and moments applied to AUV1 under the three algorithms. The blue curve represents the ASTASMC scheme, the green curve represents the traditional DLMPC scheme, and the red curve depicts the proposed DLMPC scheme. Compared with schemes (b) and (c), the control signals under the proposed scheme were regulated more swiftly, and the force and moment varied smoothly, allowing for steady trajectory tracking of the AUV formation when subjected to constraints. It is worth mentioning that the AUVs under the ASTASMC scheme required continual correction of the driving force and moment, leading to persistent chattering. This observation underscores the robustness and superiority of the FFTESO-based hierarchical DLMPC algorithm. It is noteworthy that, at the onset of the task, the proposed scheme made use of the propulsion capability to achieve the fastest possible convergence, all while adhering to the physical limitations of the thrusters. In other words, the variation

of the control signals continually remained within prescribed limits, effectively avoiding actuator saturation and reducing the failure rate.
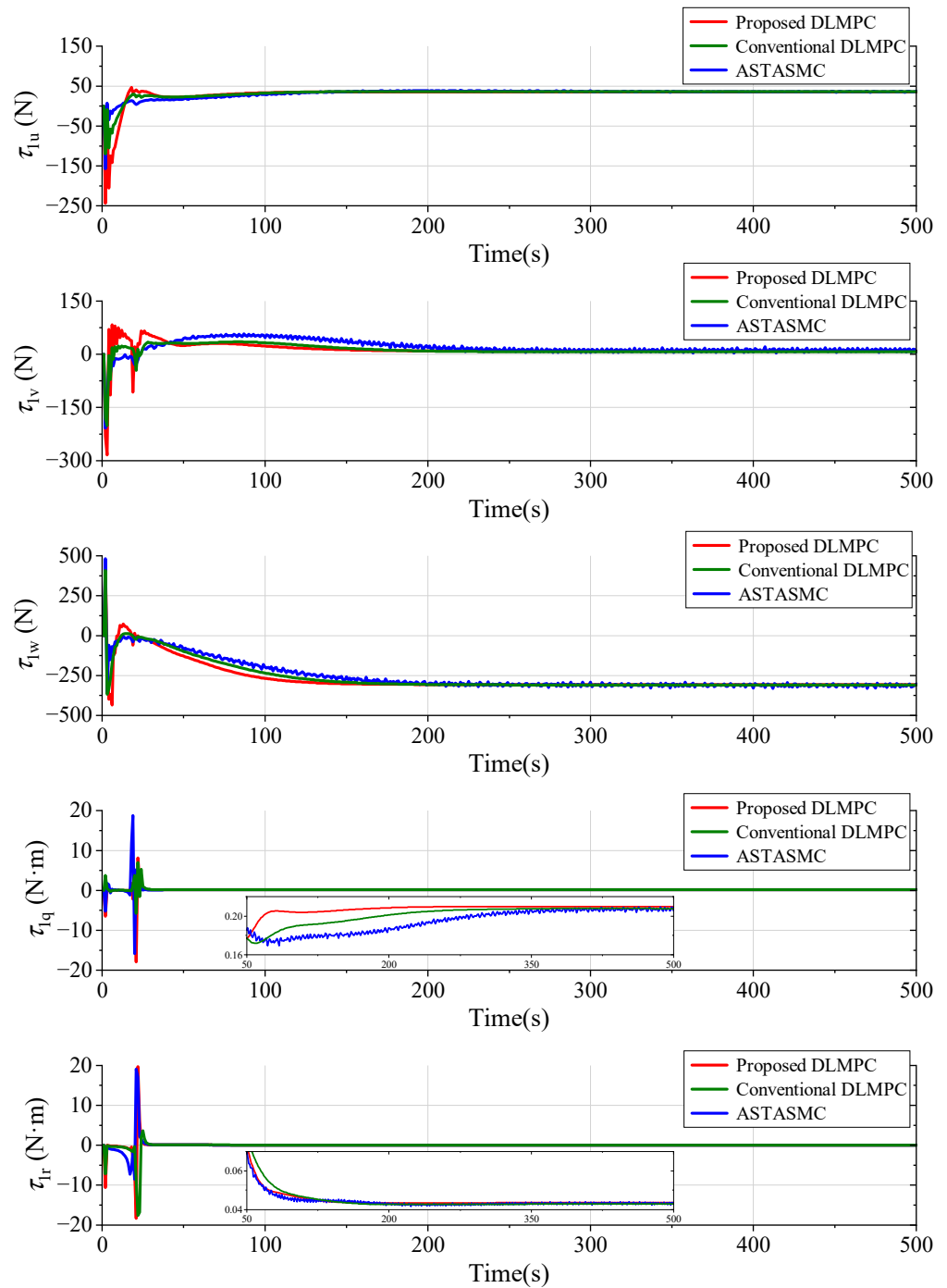
Figure 17. Actual control force and moment of AUV1.

6. Conclusions

In summary, this paper proposes a FFTESO-based hierarchical DLMPC scheme for AUV formation tracking under multiple constraints. The scheme leverages the faster and more precise compensation of lumped disturbances by FFTESO to dynamically update the prediction model online. Position tracking and velocity tracking controllers were particularly designed to determine the optimal velocities and control forces for the formation system while adhering to specified constraints. The Lyapunov-based backstepping

controllers were then employed to construct stability constraints in the DMPC optimization problem, ensuring both recursive feasibility and closed-loop stability of the control algorithm. The simulation results demonstrated that compared with the conventional DLMPC and the ASTASMC method, we enhanced the convergence speed by 31.8% and 50%, and the tracking accuracy by 38.8% and 62.1%, respectively. This demonstrates that the proposed scheme significantly improved the formation tracking performance and anti-disturbance capability. The theoretical results lay a robust foundation for the practical design and implementation of AUV formation controllers.

The main limitation of DLMPC is that it relies heavily on timely and reliable inter-subsystem communication. In the future work, we will focus on the design of a DLMPC controller for AUV formation systems subject to communication delays to overcome the communication challenges in real-world applications. In addition, in response to the issue that finite-time convergence is sensitive to the initial values of the states, we intend to investigate an extended state observer with fixed-time convergence.

Author Contributions: Conceptualization, Z.Y.; data curation, J.Z.; funding acquisition, Z.Y.; investigation, J.Z.; methodology, Z.Y. and M.Z.; resources, L.Y.; software, J.Z.; supervision, Z.Y.; validation, M.Z.; visualization, L.Y.; writing—original draft, M.Z.; writing—review and editing, M.Z. All authors have read and agreed to the published version of the manuscript.

Institutional Review Board Statement: Not applicable.

Informed Consent Statement: Not applicable.

Data Availability Statement: Data is contained within the article.

Conflicts of Interest: The authors declare no conflict of interest.

Appendix A

Proof of Theorem 1. Introducing an auxiliary error variable $\varepsilon_i^T = \left[\left(\lceil e_{i1} \rfloor^{\alpha_{i1}} + e_{i1} \right)^T, e_{i2}^T, e_{i3}^T \right]$. It can be seen that when the estimation error e_i converges to the neighborhood of the origin in finite time, ε_i also converges to the neighborhood of the origin. Taking the time derivation of ε_i, we obtain:

$$
\begin{aligned}
\dot{\varepsilon}_i &= \begin{bmatrix} \alpha_{i1}|e_{i1}|^{\alpha_{i1}-1}\dot{e}_{i1} + \dot{e}_{i1} \\ \dot{e}_{i2} \\ \dot{e}_{i3} \end{bmatrix} = \begin{bmatrix} \alpha_{i1}|e_{i1}|^{\alpha_{i1}-1}\left[e_{i2} - \beta_{i1}\left(\lceil e_{i1}\rfloor^{\alpha_{i1}} + e_{i1}\right)\right] \\ \frac{1}{2}\left[e_{i3} - \beta_{i2}\left(\lceil e_{i1}\rfloor^{\alpha_{i2}} + \gamma_i e_{i1}\right)\right] \\ -\frac{1}{2}\beta_{i3}\left(\lceil e_{i1}\rfloor^{\alpha_{i3}} + \gamma_i^2 e_{i1}\right) \end{bmatrix} \\
&\quad + \begin{bmatrix} e_{i2} - \beta_{i1}\left(\lceil e_{i1}\rfloor^{\alpha_{i1}} + e_{i1}\right) \\ \frac{1}{2}\left[e_{i3} - \beta_{i2}\left(\lceil e_{i1}\rfloor^{\alpha_{i2}} + \gamma_i e_{i1}\right)\right] \\ -\frac{1}{2}\beta_{i3}\left(\lceil e_{i1}\rfloor^{\alpha_{i3}} + \gamma_i^2 e_{i1}\right) \end{bmatrix} + \begin{bmatrix} \mathbf{0}_5 \\ \widetilde{f}_i \\ \mathbf{0}_5 \end{bmatrix} + \begin{bmatrix} \mathbf{0}_5 \\ \mathbf{0}_5 \\ -\sigma_i \end{bmatrix} \\
&= \mathrm{diag}\left(\left[|e_{i1}|^{\alpha_{i1}-1}, |e_{i1}|^{\alpha_{i1}-1}, |e_{i1}|^{\alpha_{i1}-1} \right] \right) C_{i1}\varepsilon_i + C_{i2}\varepsilon_i + F_i + \Theta_i
\end{aligned}
\tag{A1}
$$

where $F_i = \begin{bmatrix} \mathbf{0}_5 & \widetilde{f}_i & \mathbf{0}_5 \end{bmatrix}^T$, $\Theta_i = \begin{bmatrix} \mathbf{0}_5 & \mathbf{0}_5 & -\sigma_i \end{bmatrix}^T$, and the state coefficient matrices $C_{i1} = \begin{pmatrix} -\alpha_{i1}\beta_{i1}I_5 & \alpha_{i1}I_5 & \mathbf{0}_5 \\ -\beta_{i2}I_5/2 & \mathbf{0}_5 & \gamma_i^{-1}I_5/2 \\ -\beta_{i3}\gamma_i I_5/2 & \mathbf{0}_5 & \mathbf{0}_5 \end{pmatrix}$, $C_{i2} = \begin{pmatrix} -\beta_{i1}I_5 & I_5 & \mathbf{0}_5 \\ -\beta_{i2}\gamma_i I_5/2 & \mathbf{0}_5 & I_5/2 \\ -\beta_{i3}\gamma_i^2 I_5/2 & \mathbf{0}_5 & \mathbf{0}_5 \end{pmatrix}$, defining the state function $\widetilde{f}_i = f_i(z_{i2})z_{i2} - f_i\left(\hat{z}_{i2}\right)\hat{z}_{i2} = -f_i(z_{i2})e_{i2} - f_i(e_{i2})(z_{i2} + e_{i2})$. Then, we can further obtain $\left\| \widetilde{f}_i \right\| \leq l_{i1}\|z_{i2}\|\|e_{i2}\| + l_{i2}\|e_{i2}\|(\|z_{i2}\| + \|e_{i2}\|) \leq (l_{i1} + l_{i2})\overline{\mu}_i\|e_{i2}\| + l_{i2}\|e_{i2}\|^2$, with l_{i1} and l_{i2} as positive constants, and $\overline{\mu}_i$ as an upper bound of z_{i2} that exists due to limited velocity.

If the designed observer gain is restricted to $\beta_{i3} < 2\alpha_{i1}\beta_{i1}\beta_{i2}$, it is known that all eigenvalues of C_{i1} and C_{i2} have negative real parts. This means that the coefficient matrices C_{i1}, C_{i2} are Hurwitz matrices. So, there exist Hermitian matrices H_{i1} and H_{i2} such that the below Lyapunov equation holds:

$$\begin{cases} C_{i1}^T P_i + P_i C_{i1} = -H_{i1} \\ C_{i2}^T P_i + P_i C_{i2} = -H_{i2} \end{cases}. \tag{A2}$$

where P_i is a positive-definite symmetric matrix. Then, we select a candidate Lyapunov function as $V_{i1}(e_i) = \varepsilon_i^T P_i \varepsilon_i$, differentiating $V_{i1}(e_i)$ with respect to time, one obtains:

$$\begin{aligned} \dot{V}_{i1} &= \varepsilon_i^T \left[\mathrm{diag}\left(\left[|e_{i1}|^{\alpha_{i1}-1}, |e_{i1}|^{\alpha_{i1}-1}, |e_{i1}|^{\alpha_{i1}-1} \right] \right) \left(C_{i1}^T P_i + P_i C_{i1} \right) \right] \varepsilon_i + \varepsilon_i^T \left(C_{i2}^T P_i + P_i C_{i2} \right) \varepsilon_i + 2\varepsilon_i^T P_i (F_i + \Theta_i) \\ &\leq -|e_{i1}|_{\max}^{\alpha_{i1}-1} \varepsilon_i^T H_{i1} \varepsilon_i - \varepsilon_i^T H_{i2} \varepsilon_i + 2\|\varepsilon_i\|\|P_i\|(\|F_i\| + \|\Theta_i\|) \end{aligned} \tag{A3}$$

where $|e_{i1}|_{\max} = \max\{|e_{i11}|, \ldots, |e_{i15}|\}$. Given that $|e_{i1}|_{\max} \leq \|e_{i1}\| \leq \|\varepsilon_i\|^{1/\alpha_{i1}}$, and $\alpha_{i1} \in (2/3, 1)$, we can derive the following inequality:

$$\begin{aligned} \dot{V}_{i1} &\leq -\|\varepsilon_i\|^{\frac{\alpha_{i1}-1}{\alpha_{i1}}} \varepsilon_i^T H_{i1} \varepsilon_i - \varepsilon_i^T H_{i2} \varepsilon_i + 2\|\varepsilon_i\|\|P_i\|\|F_i\| + 2\|\varepsilon_i\|\|P_i\|\|\Theta_i\| \\ &\leq -\lambda_{\min}(H_{i1})\|\varepsilon_i\|^{3-\frac{1}{\alpha_{i1}}} - \lambda_{\min}(H_{i2})\|\varepsilon_i\|^2 + 2\|\varepsilon_i\|^2\|P_i\|[(l_{i1}+l_{i2})\bar{\mu}_i + l_{i2}\|\varepsilon_i\|] + 2\|\varepsilon_i\|\|P_i\|\|\Theta_i\|. \end{aligned} \tag{A4}$$

From $\lambda_{\min}(P_i)\|\varepsilon_i\|^2 \leq V_{i1} \leq \lambda_{\max}(P_i)\|\varepsilon_i\|^2$ we have $\lambda_{\max}(P_i)^{-1/2} V_{i1}^{1/2} \leq \|\varepsilon_i\| \leq \lambda_{\min}(P_i)^{-1/2} V_{i1}^{1/2}$. Since σ_i is supposed to be limited by $|\sigma_{ip}| \leq \bar{\sigma}_i$, we can obtain:

$$2\|\varepsilon_i\|\|P_i\|\|\Theta_i\| \leq 2\sqrt{5}\bar{\sigma}_i\|\varepsilon_i\|\|P_i\| \leq 2\sqrt{5}\bar{\sigma}_i\lambda_{\min}(P_i)^{-1/2}\|P_i\| V_{i1}^{1/2} \tag{A5}$$

Accordingly, inequality (A4) can be further derived as:

$$\begin{aligned} \dot{V}_{i1} &\leq -\lambda_{\min}(H_{i1})\lambda_{\max}(P_i)^{\frac{1}{2\alpha_{i1}}-\frac{3}{2}} V_{i1}^{\frac{3}{2}-\frac{1}{2\alpha_{i1}}} + 2l_{i2}\|P_i\|\lambda_{\min}(P_i)^{-\frac{3}{2}} V_{i1}^{\frac{3}{2}} + 2\sqrt{5}\bar{\sigma}_i\|P_i\|\lambda_{\min}(P_i)^{-\frac{1}{2}} V_{i1}^{\frac{1}{2}} \\ &\quad + \left(-\lambda_{\min}(H_{i2})\lambda_{\max}(P_i)^{-1} + 2(l_{i1}+l_{i2})\bar{\mu}_i\|P_i\|\lambda_{\min}(P_i)^{-1} \right) V_{i1} \\ &\leq -\lambda_{i1} V_{i1}^{\frac{3}{2}-\frac{1}{2\alpha_{i1}}} + \lambda_{i2} V_{i1} + \lambda_{i3} V_{i1}^{\frac{3}{2}} + \lambda_{i4} V_{i1}^{\frac{1}{2}} \end{aligned} \tag{A6}$$

with $\lambda_{i1} = -\lambda_{\min}(H_{i1})\lambda_{\max}(P_i)^{\frac{1}{2\alpha_{i1}}-\frac{3}{2}}$, $\lambda_{i2} = -\lambda_{\min}(H_{i2})\lambda_{\max}(P_i)^{-1} + 2(l_{i1}+l_{i2})\bar{\mu}_i\|P_i\|\lambda_{\min}(P_i)^{-1}$, $\lambda_{i3} = 2l_{i2}\|P_i\|\lambda_{\min}(P_i)^{-\frac{3}{2}}$ and $\lambda_{i4} = 2\sqrt{5}\bar{\sigma}_i\|P_i\|\lambda_{\min}(P_i)^{-\frac{1}{2}}$. Then, we define two new variables as $\bar{\lambda}_{i2} = \lambda_{i2} V_{i1}(e_i^0)^{-\frac{1}{2}+\frac{1}{2\alpha_{i1}}}$, $\bar{\lambda}_{i3} = \lambda_{i3} V_{i1}(e_i^0)^{\frac{1}{2\alpha_{i1}}}$, and a restriction region Θ_{i1} specified for the initial value $V_{i1}(e_i^0)$. For $e_i \in \Theta_{i1} = \left\{ e_i | \lambda_{i2} V_{i1}^{-\frac{1}{2}+\frac{1}{2\alpha_{i1}}} + \lambda_{i3} V_{i1}^{\frac{1}{2\alpha_{i1}}} < \lambda_{i1} \right\}$, there is $\dot{V}_{i1} < 0$. This indicates that V_{i1} is a monotonically decreasing function, then it has $V_{i1}(e_i^0) \geq V_{i1}(e_i)$, and $\bar{\lambda}_{i2} + \bar{\lambda}_{i3} < \lambda_{i1}$. According to the above definition, inequality (A6) can be simplified as:

$$\begin{aligned} \dot{V}_{i1} &\leq -(\lambda_{i1} - \bar{\lambda}_{i2} - \bar{\lambda}_{i3}) V_{i1}^{\frac{3}{2}-\frac{1}{2\alpha_{i1}}} + \lambda_{i2} V_{i1} - \bar{\lambda}_{i2} V_{i1}^{\frac{3}{2}-\frac{1}{2\alpha_{i1}}} + \lambda_{i3} V_{i1}^{\frac{3}{2}} - \bar{\lambda}_{i3} V_{i1}^{\frac{3}{2}-\frac{1}{2\alpha_{i1}}} + \lambda_{i4} V_{i1}^{\frac{1}{2}} \\ &\leq -(\lambda_{i1} - \bar{\lambda}_{i2} - \bar{\lambda}_{i3}) V_{i1}^{\frac{3}{2}-\frac{1}{2\alpha_{i1}}} + \lambda_{i4} V_{i1}^{\frac{1}{2}} = -\lambda_{i5} V_{i1}^{\frac{3}{2}-\frac{1}{2\alpha_{i1}}} + \lambda_{i4} V_{i1}^{\frac{1}{2}} \end{aligned} \tag{A7}$$

where $\lambda_{i5} = \lambda_{i1} - \bar{\lambda}_{i2} - \bar{\lambda}_{i3}$, it can be noted that the inequality (A7) has the same structure as Proposition 2 of [41]. Therefore, the error trajectory of the designed FTESO (8) is finite-time uniformly ultimately bounded stable, which means that the estimation errors e_i will

converge to a small neighborhood of the origin. Furthermore, the convergence time T_{if} is given by:

$$T_{if} \leq \frac{2\alpha_{i1} V_{i1}\left(e_i^0\right)^{\frac{1}{2\alpha_{i1}} - \frac{1}{2}}}{(\lambda_{i5} - \delta_{i5})(1 - \alpha_{i1})}. \tag{A8}$$

With the stable region Ω_i given by $\Omega_i = \left\{ e_i | V_{i1}(e_i)^{1 - \frac{1}{2\alpha_{i1}}} < \lambda_{i4}/\delta_{i5} \right\}$, where $\delta_{i5} \in (0, \lambda_{i5})$ is an arbitrary constant. This completes the proof. $\square$

Appendix B

Proof of Theorem 2. Given the current system state $x_{i1}(t)$, if $\left\| u_{i1}^{vir}\left(\widehat{x}_{i1}\right) \right\|_\infty \leq u_{i1}^{\max}$ can be satisfied, then $u_{i1}^{vir}\left(\widehat{x}_{i1}\right)$ is always feasible for the DLMPC optimization problem (11).

Taking the infinity norm on both sides of (14), we have

$$
\begin{aligned}
\left\| v_i^{vir}\left(\widehat{x}_{i1}\right) \right\|_\infty &= \left\| J_i^{-1}(\eta_i) \right\|_\infty \left\| \dot{\eta}_r - K_{ip}\tilde{\eta}_i \right\|_\infty \leq \left\| J_i^{-1}(\eta_i) \right\|_\infty \left(\|\dot{\eta}_r\|_\infty + \left\| K_{ip}\tilde{\eta}_i \right\|_\infty \right) \\
&\leq \left\| J_i^{-1}(\eta_i) \right\|_\infty \left(\overline{\eta}_{r1} + \overline{K}_{ip}\left\| \tilde{\eta}_i \right\|_\infty \right).
\end{aligned} \tag{A9}
$$

From (15), $\dot{V}_{ip} \leq 0$. Therefore, $\left\| \tilde{\eta}_i(t) \right\| \leq \left\| \tilde{\eta}_i(0) \right\|$. Considering that $\left\| \tilde{\eta}_i \right\|_\infty \leq \left\| \tilde{\eta}_i \right\|$, we have $\left\| \tilde{\eta}_i \right\|_\infty \leq \left\| \tilde{\eta}_i(0) \right\|$. According to the property of the rotation matrix (3), we obtain

$$
\begin{aligned}
\left\| J_i^{-1}(\eta_i) \right\|_\infty = \max\{ &|\cos\psi_i\cos\theta_i| + |\sin\psi_i\cos\theta_i| + |-\sin\theta_i|, \ |-\sin\psi_i| + |\cos\psi_i|, \\
&|\cos\psi_i\sin\theta_i| + |\sin\psi_i\sin\theta_i| + |\cos\theta_i|, \ 1, \ |1/\cos\theta_i| \} \leq 1 + \frac{\sqrt{2}}{2}.
\end{aligned} \tag{A10}
$$

Accordingly, (A9) can be further derived as:

$$\left\| v_i^{vir}\left(\widehat{x}_{i1}\right) \right\|_\infty \leq \left(1 + \frac{\sqrt{2}}{2}\right)\left(\overline{\eta}_{r1} + \overline{K}_{ip}\left\| \tilde{\eta}_i(0) \right\|\right). \tag{A11}$$

If (24) can be satisfied, then the relation $\left\| v_i^{vir}\left(\widehat{x}_{i1}\right) \right\|_\infty \leq v_i^{\max}$ can hold. This ensures that $\left\| u_{i1}^{vir}\left(\widehat{x}_{i1}\right) \right\|_\infty \leq u_{i1}^{\max}$ holds at all moments, which concludes the proof. $\square$

Appendix C

Proof of Theorem 3. Given the current system state $x_{i2}(t)$, if $\left\| \widehat{u}_{i2}^{vir}\left(\widehat{x}_{i2}\right) \right\|_\infty \leq u_{i2}^{\max}$ can be satisfied, then $\widehat{u}_{i2}^{vir}\left(\widehat{x}_{i2}\right)$ is always feasible for the DLMPC optimization problem (18).

Consider the following Lyapunov function:

$$V_i = V_{iv} + V_{i1} = \frac{1}{2}\gamma_i^T \Pi_i \gamma_i \tag{A12}$$

where $\gamma_i = \left[\tilde{\eta}_i^T, \tilde{v}_i^T, \sqrt{2}\varepsilon_i^T\right]^T$, $\Pi_i = \mathrm{diag}(\Lambda_{i1}, \Lambda_{i2}, P_i)$. From (22) and the proof of Theorem 1, it follows that $\dot{V}_i \leq 0$. Therefore, $\|\gamma_i(t)\| \leq \|\gamma_i(0)\|$. Moreover, we have $\left\| \tilde{\eta}_i \right\|_\infty \leq$

$\left\|\tilde{\boldsymbol{\eta}}_i\right\| \leq \|\boldsymbol{\gamma}_i\|$, $\left\|\tilde{\boldsymbol{v}}_i\right\|_\infty \leq \left\|\tilde{\boldsymbol{v}}_i\right\| \leq \|\boldsymbol{\gamma}_i\|$, $\|\boldsymbol{\varepsilon}_i\|_\infty < \left\|\sqrt{2}\boldsymbol{\varepsilon}_i\right\|_\infty \leq \left\|\sqrt{2}\boldsymbol{\varepsilon}_i\right\| \leq \|\boldsymbol{\gamma}_i\|$, then $\left\|\tilde{\boldsymbol{\eta}}_i\right\|_\infty \leq$ $\|\boldsymbol{\gamma}_i(0)\|$, $\left\|\tilde{\boldsymbol{v}}_i\right\|_\infty \leq \|\boldsymbol{\gamma}_i(0)\|$, and $\|\boldsymbol{\varepsilon}_i\|_\infty \leq \|\boldsymbol{\gamma}_i(0)\|$.

Since the desired speed in the velocity tracking controller is derived from the position controller, we have $\dot{\boldsymbol{v}}_{id} = \dot{\boldsymbol{u}}_{i1} = [\boldsymbol{v}_i(t+h) - \boldsymbol{v}_i(t)]/h$. Then, we take the infinity norm on $\dot{\boldsymbol{v}}_{id}$ to obtain:

$$
\begin{aligned}
\|\dot{\boldsymbol{v}}_{id}\|_\infty &= \left\|\frac{\boldsymbol{v}_i(t+h) - \boldsymbol{v}_i(t)}{h}\right\|_\infty \leq \frac{\|\boldsymbol{v}_i(t+h)\|_\infty + \|\boldsymbol{v}_i(t)\|_\infty}{h} \leq \frac{2\|\boldsymbol{v}_i\|_\infty}{h} \\
&\leq \frac{2\left\|\boldsymbol{v}_i^{vir}\left(\widehat{\boldsymbol{x}}_{i1}\right)\right\|_\infty}{h} \leq \frac{2+\sqrt{2}}{h}\left(\overline{\eta}_{r1} + \overline{K}_{ip}\|\boldsymbol{\gamma}_i(0)\|\right) = \overline{v}_{id}
\end{aligned}
\tag{A13}
$$

where $\|\boldsymbol{v}_i\|_\infty \leq \left\|\boldsymbol{v}_i^{vir}\left(\widehat{\boldsymbol{x}}_{i1}\right)\right\|_\infty \leq \left(1 + \frac{\sqrt{2}}{2}\right)\left(\overline{\eta}_{r1} + \overline{K}_{ip}\|\boldsymbol{\gamma}_i(0)\|\right) = \overline{v}_i$. Consequently, the bound of the Coriolis and centripetal matrix $\boldsymbol{C}_i^*(\boldsymbol{v}_i)$ can be obtained by taking the infinity norm:

$$
\|\boldsymbol{C}_i^*(\boldsymbol{v}_i)\|_\infty \leq \left(2 + \sqrt{2}\right)\overline{m}_i\left(\overline{\eta}_{r1} + \overline{K}_{ip}\|\boldsymbol{\gamma}_i(0)\|\right) = \overline{c}_i
\tag{A14}
$$

$\|\boldsymbol{D}_i^*(\boldsymbol{v}_i)\|_\infty$ can be derived by the same principle:

$$
\|\boldsymbol{D}_i^*(\boldsymbol{v}_i)\|_\infty \leq \overline{d}_1 + \overline{d}_2\left(1 + \frac{\sqrt{2}}{2}\right)\left(\overline{\eta}_{r1} + \overline{K}_{ip}\|\boldsymbol{\gamma}_i(0)\|\right) = \overline{d}_i
\tag{A15}
$$

with $\overline{d}_1 = \max\{|X_u|, |Y_v|, |Z_w|, |M_q|, |N_r|\}$, $\overline{d}_2 = \max\left\{X_{|u|u}, Y_{|v|v}, Z_{|w|w}, M_{|q|q}, N_{|r|r}\right\}$. Taking infinity norms on both sides of the lumped disturbance $\widehat{\boldsymbol{\tau}}_{id} = \boldsymbol{M}_i^* \boldsymbol{J}_i^{-1}(\boldsymbol{\eta}_i)\widehat{\boldsymbol{d}}_i$, one obtains:

$$
\begin{aligned}
\left\|\widehat{\boldsymbol{\tau}}_{id}\right\|_\infty &= \left\|\boldsymbol{M}_i^* \boldsymbol{J}_i^{-1}(\boldsymbol{\eta}_i)\widehat{\boldsymbol{d}}_i\right\|_\infty = \left\|\boldsymbol{M}_i^* \boldsymbol{J}_i^{-1}(\boldsymbol{\eta}_i)(\boldsymbol{d}_i + \boldsymbol{e}_{i3})\right\|_\infty \leq \|\boldsymbol{\tau}_{id}\|_\infty + \left\|\boldsymbol{M}_i^* \boldsymbol{J}_i^{-1}(\boldsymbol{\eta}_i)\right\|_\infty \|\boldsymbol{e}_{i3}\|_\infty \\
&\leq \|\boldsymbol{\tau}_{id}\| + \left(1 + \frac{\sqrt{2}}{2}\right)\overline{m}_i\|\boldsymbol{\varepsilon}_i\|_\infty \leq \overline{\tau}_{id} + \left(1 + \frac{\sqrt{2}}{2}\right)\overline{m}_i\|\boldsymbol{\gamma}_i(0)\|.
\end{aligned}
\tag{A16}
$$

Based on the above analysis, taking the infinity norms on both sides of (21) yields:

$$
\begin{aligned}
\left\|\boldsymbol{\tau}_i^{vir}\left(\widehat{\boldsymbol{x}}_{i2}\right)\right\|_\infty &= \|\boldsymbol{C}_i^*(\boldsymbol{v}_i)\boldsymbol{v}_i + \boldsymbol{D}_i^*(\boldsymbol{v}_i)\boldsymbol{v}_i\|_\infty + \|\boldsymbol{M}_i^* \dot{\boldsymbol{v}}_{id}\|_\infty + \left\|\boldsymbol{M}_i^* \boldsymbol{K}_{iv}\tilde{\boldsymbol{v}}_i\right\|_\infty + \left\|\widehat{\boldsymbol{\tau}}_{id}\right\|_\infty \\
&\leq \left(\overline{c}_i + \overline{d}_i\right)\|\boldsymbol{v}_i\|_\infty + \overline{m}_i\|\dot{\boldsymbol{v}}_{id}\|_\infty + \overline{m}_i\overline{K}_{iv}\left\|\tilde{\boldsymbol{v}}_i\right\|_\infty + \left\|\widehat{\boldsymbol{\tau}}_{id}\right\|_\infty \\
&\leq \left(\overline{c}_i + \overline{d}_i\right)\overline{v}_i + \overline{m}_i\overline{v}_{id} + \left[\overline{K}_{iv} + \left(1 + \frac{\sqrt{2}}{2}\right)\right]\overline{m}_i\|\boldsymbol{\gamma}_i(0)\| + \overline{\tau}_{id}.
\end{aligned}
\tag{A17}
$$

If (25) can be satisfied, then the relation $\left\|\boldsymbol{\tau}_i^{vir}\left(\widehat{\boldsymbol{x}}_{i2}\right)\right\|_\infty \leq \tau_i^{\max}$ can hold. This ensures that $\left\|\widehat{\boldsymbol{u}}_{i2}^{vir}\left(\widehat{\boldsymbol{x}}_{i2}\right)\right\|_\infty \leq u_{i2}^{\max}$ holds at all moments, which concludes the proof. $\square$

Appendix D

Proof of Theorem 4. Since we have constructed a Lyapunov function $V_{ip}(\boldsymbol{x}_{i1})$ that is continuously differentiable and radically unbounded, according to converse Lyapunov theorems [42], there exist functions $\chi_{ik}(\cdot)$ (k = 1, 2, 3) belonging to class $\mathcal{K}_\infty$ that satisfy the following inequalities:

$$
\chi_{i1}(\|\boldsymbol{x}_{i1}\|) \leq V_{ip}(\boldsymbol{x}_{i1}) \leq \chi_{i2}(\|\boldsymbol{x}_{i1}\|)
\tag{A18}
$$

$$\dot{V}_{ip}\Big|_{\boldsymbol{u}_{i1}^{vir}(\boldsymbol{x}_{i1})} \leq -\chi_{i3}(\|\boldsymbol{x}_{i1}\|) \tag{A19}$$

In view of the stability constraint (11f) and the optimal solution $\boldsymbol{\kappa}_{i1}(s)$ implemented at each sampling period, we obtain:

$$\dot{V}_{ip}\Big|_{\boldsymbol{u}_{i1}(\boldsymbol{x}_{i1})} \leq \dot{V}_{ip}\Big|_{\boldsymbol{u}_{i1}^{vir}(\boldsymbol{x}_{i1})} \leq -\chi_{i3}(\|\boldsymbol{x}_{i1}\|). \tag{A20}$$

From the Lyapunov argument of Theorem 4.8 in [42], we conclude that the position tracking subsystem is asymptotically stable within an attraction region $\mathcal{R}_{i1}$.

$$\left\{ \boldsymbol{x}_{i1} \in \mathcal{R}_{i1}^n \middle| \left(1 + \frac{\sqrt{2}}{2}\right)\left(\overline{\eta}_{r1} + \overline{K}_{ip}\left\|\tilde{\boldsymbol{\eta}}_i(0)\right\|\right) \leq v_i^{\max} \right\}. \tag{A21}$$

Similarly, the following conclusion can be obtained: the velocity tracking subsystem under Algorithm 1 is asymptotically stable within an attraction region $\mathcal{R}_{i2}$.

$$\left\{ \boldsymbol{x}_{i2} \in \mathcal{R}_{i2}^n \middle| \left(\overline{c}_i + \overline{d}_i\right)\overline{v}_i + \overline{m}_i\overline{v}_{id} + \left[\overline{K}_{iv} + \left(1 + \frac{\sqrt{2}}{2}\right)\right]\overline{m}_i\|\gamma_i(0)\| + \overline{\tau}_{id} \leq \tau_i^{\max} \right\}. \tag{A22}$$

This ensures the stability of the overall AUV formation system. Since there are no other limitations on $\overline{K}_{ip}$ and $\overline{K}_{iv}$, the attraction regions $\mathcal{R}_{i1}$ and $\mathcal{R}_{i2}$ can be arbitrarily large as long as the control gains are small enough. $\square$

Remark A1. *It is noteworthy that the tracking control performance of the backstepping technique-based virtual control law relies on the amplitude of the control gains. As seen in (14) and (21), smaller values of $\overline{K}_{ip}$ and $\overline{K}_{iv}$ result in slower convergence. Moreover, thanks to the optimization process of the proposed DLMPC controller, even if smaller control gains are chosen to expand the attractive regions, the controller can effectively leverage the thrust capability to achieve optimal control performance aligned with the cost function. This confirms the advantage that DLMPC inherits the stability properties of the virtual controller.*

References

1. Shi, Y.; Shen, C.; Fang, H.; Li, H. Advanced control in marine mechatronic systems: A survey. *IEEE-ASME Trans. Mechatron.* **2017**, *22*, 1121–1131. [CrossRef]
2. Wang, C.; Cai, W.; Lu, J.; Ding, X.; Yang, J. Design, modeling, control, and experiments for multiple AUVs formation. *IEEE Trans. Autom. Sci. Eng.* **2021**, *19*, 2776–2787. [CrossRef]
3. Yu, H.; Zeng, Z.; Guo, C. Coordinated formation control of discrete-time autonomous underwater vehicles under alterable communication topology with time-varying delay. *J. Mar. Sci. Eng.* **2022**, *10*, 712. [CrossRef]
4. Chen, G.; Shen, Y.; Qu, N.; He, B. Path planning of AUV during diving process based on behavioral decision-making. *Ocean Eng.* **2021**, *234*, 109073. [CrossRef]
5. Cui, R.; Ge, S.S.; How, B.V.E.; Choo, Y.S. Leader–follower formation control of underactuated autonomous underwater vehicles. *Ocean Eng.* **2010**, *37*, 1491–1502. [CrossRef]
6. He, X.; Geng, Z. Globally convergent leaderless formation control for unicycle-type mobile robots. *IET Control Theory Appl.* **2020**, *14*, 2651–2662. [CrossRef]
7. Zhen, Q.; Wan, L.; Li, Y.; Jiang, D. Formation control of a multi-AUVs system based on virtual structure and artificial potential field on SE(3). *Ocean Eng.* **2022**, *253*, 111148. [CrossRef]
8. Hu, C.D.; Wu, D.F.; Liao, Y.X.; Hu, X. Sliding mode control unified with the uncertainty and disturbance estimator for dynamically positioned vessels subjected to uncertainties and unknown disturbances. *Appl. Ocean Res.* **2021**, *109*, 102564. [CrossRef]
9. Zhang, W.; Wu, W.; Li, Z.; Du, X.; Yan, Z. Three-Dimensional Trajectory Tracking of AUV Based on Nonsingular Terminal Sliding Mode and Active Disturbance Rejection Decoupling Control. *J. Mar. Sci. Eng.* **2023**, *11*, 959. [CrossRef]
10. Peng, Z.; Wang, J.; Wang, J. Constrained control of autonomous underwater vehicles based on command optimization and disturbance estimation. *IEEE Trans. Ind. Electron.* **2018**, *66*, 3627–3635. [CrossRef]
11. Miao, J.; Sun, X.; Chen, Q.; Zhang, H.; Liu, W.; Wang, Y. Robust Path-Following Control for AUV under Multiple Uncertainties and Input Saturation. *Drones* **2023**, *7*, 665. [CrossRef]

12. Zhang, Y.; Liu, X.; Luo, M.; Yang, C. MPC-based 3-D trajectory tracking for an autonomous underwater vehicle with constraints in complex ocean environments. *Ocean Eng.* **2019**, *189*, 106309. [CrossRef]

13. Yong, K.; Chen, M.; Wu, Q. Anti-disturbance control for nonlinear systems based on interval observer. *IEEE Trans. Ind. Electron.* **2019**, *67*, 1261–1269. [CrossRef]

14. Chen, C.; Wen, C.; Liu, Z.; Xie, K.; Zhang, Y.; Chen, C.P. Adaptive consensus of nonlinear multi-agent systems with non-identical partially unknown control directions and bounded modelling errors. *IEEE Trans. Autom. Control.* **2016**, *62*, 4654–4659. [CrossRef]

15. Guo, P.; Lyu, M.R.; Chen, C.L.P. Regularization parameter estimation for feedforward neural networks. *IEEE Trans. Syst. Man Cybern. Part B-Cybern.* **2003**, *33*, 35–44.

16. Han, J. From PID to active disturbance rejection control. *IEEE Trans. Ind. Electron.* **2009**, *56*, 900–906. [CrossRef]

17. Fernandes, D.D.A.; Sørensen, A.J.; Pettersen, K.Y.; Donha, D.C. Output feedback motion control system for observation class ROVs based on a high-gain state observer: Theoretical and experimental results. *Control Eng. Pract.* **2015**, *39*, 90–102. [CrossRef]

18. Lamraoui, H.C.; Qidan, Z. Path following control of fully-actuated autonomous underwater vehicle in presence of fast-varying disturbances. *Appl. Ocean Res.* **2019**, *86*, 40–46. [CrossRef]

19. Basin, M.; Yu, P.; Shtessel, Y. Finite-and fixed-time differentiators utilising HOSM techniques. *IET Control Theory Appl.* **2017**, *11*, 1144–1152. [CrossRef]

20. Li, B.; Hu, Q.; Yang, Y. Continuous finite-time extended state observer based fault tolerant control for attitude stabilization. *Aerosp. Sci. Technol.* **2019**, *84*, 204–213. [CrossRef]

21. Cai, X.; Zhu, X.; Yao, W. FTESO-adaptive neural network based safety control for a quadrotor UAV under multiple disturbances: Algorithm and experiments. *Int. J. Robot. Res. Appl.* **2024**, *51*, 20–33. [CrossRef]

22. Xia, Y.; Xu, K.; Huang, Z.; Wang, W.; Xu, G.; Li, Y. Adaptive energy-efficient tracking control of a X rudder AUV with actuator dynamics and rolling restriction. *Appl. Ocean Res.* **2022**, *118*, 102994. [CrossRef]

23. Xia, G.; Zhang, Y.; Zhang, W.; Zhang, K.; Yang, H. Robust adaptive super-twisting sliding mode formation controller for homing of multi-underactuated AUV recovery system with uncertainties. *ISA Trans.* **2022**, *130*, 136–151. [CrossRef]

24. Li, H.; Xie, P.; Yan, W. Receding horizon formation tracking control of constrained underactuated autonomous underwater vehicles. *IEEE Trans. Ind. Electron.* **2016**, *64*, 5004–5013. [CrossRef]

25. Zhang, M.; Yan, Z.; Zhou, J.; Yue, L. Distributed Dual Closed-Loop Model Predictive Formation Control for Collision-Free Multi-AUV System Subject to Compound Disturbances. *J. Mar. Sci. Eng.* **2023**, *11*, 1897. [CrossRef]

26. Liu, C.; Sun, T.; Hu, Q.Z. Synchronization Control of Dynamic Positioning Ships Using Model Predictive Control. *J. Mar. Sci. Eng.* **2021**, *9*, 1239. [CrossRef]

27. Shen, C.; Shi, Y.; Buckham, B. Trajectory tracking control of an autonomous underwater vehicle using Lyapunov-based model predictive control. *IEEE Trans. Ind. Electron.* **2017**, *65*, 5796–5805. [CrossRef]

28. Mahmood, M.; Mhaskar, P. Lyapunov-based model predictive control of stochastic nonlinear systems. *Automatica* **2012**, *48*, 2271–2276. [CrossRef]

29. Liu, J.; Chen, X.; de la Pena, D.M.M.; Christofides, P.D. Iterative distributed model predictive control of nonlinear systems: Handling asynchronous, delayed measurements. *IEEE Trans. Autom. Control* **2011**, *57*, 528–534.

30. Wei, H.; Shen, C.; Shi, Y. Distributed Lyapunov-based model predictive formation tracking control for autonomous underwater vehicles subject to disturbances. *IEEE Trans. Syst. Man Cybern. Syst.* **2019**, *51*, 5198–5208. [CrossRef]

31. Meng, C.; Zhang, W.; Du, X. Finite-time extended state observer based collision-free leaderless formation control of multiple AUVs via event-triggered control. *Ocean Eng.* **2023**, *268*, 113605. [CrossRef]

32. Yan, Z.; Gong, P.; Zhang, W.; Li, Z.; Teng, Y. Autonomous underwater vehicle vision guided docking experiments based on L-shaped light array. *IEEE Access* **2019**, *7*, 72567–72576. [CrossRef]

33. Fossen, T.I. *Handbook of Marine Craft Hydrodynamics and Motion Control*; John Wiley & Sons: Hoboken, NJ, USA, 2011.

34. Xu, J.; Cui, Y.; Xing, W.; Huang, F.; Yan, Z.; Wu, D.; Chen, T. Anti-disturbance fault-tolerant formation containment control for multiple autonomous underwater vehicles with actuator faults. *Ocean Eng.* **2022**, *266*, 112924. [CrossRef]

35. Zhang, Z.; Lin, M.; Li, D. A double-loop control framework for AUV trajectory tracking under model parameters uncertainties and time-varying currents. *Ocean Eng.* **2022**, *265*, 112566. [CrossRef]

36. Chen, C.W.; Lu, Y.F. Computational fluid dynamics study of water entry impact forces of an airborne-launched, axisymmetric, disk-type Autonomous underwater hovering vehicle. *Symmetry* **2019**, *11*, 1100. [CrossRef]

37. Cui, R.; Chen, L.; Yang, C.; Chen, M. Extended state observer-based integral sliding mode control for an underwater robot with unknown disturbances and uncertain nonlinearities. *IEEE Trans. Ind. Electron.* **2017**, *64*, 6785–6795. [CrossRef]

38. Majeed, A.; Rauf, I. Graph Theory: A Comprehensive Survey about Graph Theory Applications in Computer Science and Social Networks. *Inventions* **2020**, *5*, 10. [CrossRef]

39. Liu, J.; de la Peña, D.M.; Christofides, P.D. Distributed model predictive control of nonlinear systems subject to asynchronous and delayed measurements. *Automatica* **2010**, *46*, 52–61. [CrossRef]

40. Yan, Z.; Wang, M.; Xu, J. Integrated guidance and control strategy for homing of unmanned underwater vehicles. *J. Frankl. Inst.-Eng. Appl. Math.* **2019**, *356*, 3831–3848. [CrossRef]

41. Hu, Q.; Jiang, B. Continuous finite-time attitude control for rigid spacecraft based on angular velocity observer. *IEEE Trans. Aerosp. Electron. Syst.* **2018**, *54*, 1082–1092. [CrossRef]
42. Khalil, H.K. *Nonlinear Systems*; Prentice Hall Inc.: Upper Saddle River, NJ, USA, 2002.